

BIFURCATION ANALYSIS OF A GENERAL CLASS OF NONLINEAR INTEGRATE-AND-FIRE NEURONS*

JONATHAN TOUBOUL†

Abstract. In this paper we define a class of formal neuron models being computationally efficient and biologically plausible, i.e., able to reproduce a wide range of behaviors observed in *in vivo* or *in vitro* recordings of cortical neurons. This class includes, for instance, two models widely used in computational neuroscience, the Izhikevich and the Brette–Gerstner models. These models consist of a 4-parameter dynamical system. We provide the full local bifurcation diagram of the members of this class and show that they all present the same bifurcations: an Andronov–Hopf bifurcation manifold, a saddle-node bifurcation manifold, a Bogdanov–Takens bifurcation, and possibly a Bautin bifurcation, i.e., all codimension two local bifurcations in a two-dimensional phase space except the cusp. Among other global bifurcations, this system shows a saddle homoclinic bifurcation curve. We show how this bifurcation diagram generates the most prominent cortical neuron behaviors. This study leads us to introduce a new neuron model, the *quartic model*, able to reproduce among all the behaviors of the Izhikevich and Brette–Gerstner models self-sustained subthreshold oscillations, which are of great interest in neuroscience.

Key words. neuron models, dynamical system analysis, nonlinear dynamics, Hopf bifurcation, saddle-node bifurcation, Bogdanov–Takens bifurcation, Bautin bifurcation, saddle homoclinic bifurcation, subthreshold neuron oscillations

AMS subject classifications. 34C05, 34C23, 34C60, 92B20, 92C20

DOI. 10.1137/070687268

Introduction. During the past few years, in the neurocomputing community, the problem of finding a computationally simple and biologically realistic model of neuron has been widely studied, in order to be able to compare experimental recordings with numerical simulations of large-scale brain models. The key problem is to find a model of neuron realizing a compromise between its simulation efficiency and its ability to reproduce what is observed at the cell level, often considering *in-vitro* experiments [15, 18, 24].

Among the numerous neuron models, from the detailed Hodgkin–Huxley model [11] still considered as the reference, but unfortunately computationally intractable when considering neuronal networks, down to the simplest integrate-and-fire model [8] very effective computationally, but unrealistically simple and unable to reproduce many behaviors observed, two models seem to stand out [15]: the adaptive quadratic (Izhikevich [14] and related models such as the theta model with adaptation [6, 10]) and exponential (Brette and Gerstner [5]) neuron models. These two models are computationally almost as efficient as the integrate-and-fire model. The Brette–Gerstner model involves an exponential function, which needs to be tabulated if we want the algorithm to be efficient. They are also biologically plausible, and reproduce several important neuronal regimes with a good adequacy with biological data, especially in high-conductance states, typical of cortical *in vivo* activity. Nevertheless, they fail in reproducing deterministic self-sustained subthreshold oscillations, a behavior of particular interest in cortical neurons for the precision and robustness of spike generation

*Received by the editors April 2, 2007; accepted for publication (in revised form) November 12, 2007; published electronically February 29, 2008.

<http://www.siam.org/journals/siap/68-4/68726.html>

†Odyssee Laboratory, INRIA/ENPC/ENS, INRIA, Sophia-Antipolis, 2004 route des Lucioles, BP 93 06902, Sophia-Antipolis Cedex, France (jonathan.touboul@sophia.inria.fr).

patterns, for instance in the inferior olive nucleus [4, 22, 23], in the stellate cells of the entorhinal cortex [1, 2, 17], and in the dorsal root ganglia (DRG) [3, 20, 21]. Some models have been introduced to study from a theoretical point of view the currents involved in the generation of self-sustained subthreshold oscillations [25], but the model failed in reproducing lots of other neuronal behaviors.

The aim of this paper is to define and study a general class of neuron models, containing the Izhikevich and Brette–Gerstner models, from a dynamical systems point of view. We characterize the local bifurcations of these models and show how their bifurcations are linked with different biological behaviors observed in the cortex. This formal study will lead us to define a new model of neuron, whose behaviors include those of the Izhikevich–Brette–Gerstner (IBG) models but also self-sustained subthreshold oscillations.

In the first section of this paper, we introduce a general class of nonlinear neuron models which contains the IBG models. We study the fixed-point bifurcation diagram of the elements of this class, and show that they present the same local bifurcation diagram, with a saddle-node bifurcation curve, an Andronov–Hopf bifurcation curve, a Bogdanov–Takens bifurcation point, and possibly a Bautin bifurcation, i.e., all codimension two bifurcations in dimension two except the cusp. This analysis is applied in the second section to the Izhikevich and the Brette–Gerstner models. We derive their bifurcation diagrams and prove that none of them shows the Bautin bifurcation. In the third section, we introduce a new simple model—the *quartic model*—presenting, in addition to common properties of the dynamical system of this class, a Bautin bifurcation, which can produce self-sustained oscillations. Last, the fourth section is dedicated to numerical experiments. We show that the quartic model is able to reproduce some of the prominent features of biological spiking neurons. We give qualitative interpretations of those different neuronal regimes from the dynamical systems point of view, in order to give a grasp of how the bifurcations generate biologically plausible behaviors. We also show that the new quartic model, presenting supercritical Hopf bifurcations, is able to reproduce the oscillatory/spiking behavior presented, for instance, in the DRG. Finally, we show that numerical simulation results of the quartic model show a good agreement with biological intracellular recordings in the DRG.

1. Bifurcation analysis of a class of nonlinear neuron models. In this section we introduce a large class of formal neurons which are able to reproduce a wide range of neuronal behaviors observed in cortical neurons. This class of models is inspired by the review made by Izhikevich [15]. He found that the quadratic adaptive integrate-and-fire model was able to simulate efficiently a lot of interesting behaviors. Brette and Gerstner [5] defined a similar model of neuron which presented a good adequacy between simulations and biological recordings.

We generalize these models, and define a new class of neuron models, wide but specific enough to keep the diversity of behaviors of the IBG models.

1.1. The general class of nonlinear models. In this paper, we are interested in neurons defined by a dynamical system of the type

$$\begin{cases} \frac{dv}{dt} = F(v) - w + I, \\ \frac{dw}{dt} = a(bv - w), \end{cases}$$

where a, b , and I are real parameters and F is a real function.¹

In this equation, v represents the membrane potential of the neuron, w is the adaptation variable, I represents the input intensity of the neuron, $1/a$ is the characteristic time of the adaptation variable, and b accounts for the interaction between the membrane potential and the adaptation variable.²

This equation is a very general model of neuron. For instance when F is a polynomial of degree three, we obtain a FitzHugh–Nagumo model, when F is a polynomial of degree two the Izhikevich neuron model [14], and when F is an exponential function the Brette–Gerstner model [5]. However, in contrast with continuous models like the FitzHugh–Nagumo model [8], the two latter cases diverge when spiking, and an external reset mechanism is used after a spike is emitted.

In this paper, we want this class of models to have common properties with the IBG neuron models. To this purpose, let us make some assumptions on the function F . The first assumption is a regularity assumption.

Assumption (A1). F is at least three times continuously differentiable.

A second assumption is necessary to ensure us that the system would have the same number of fixed points as the IBG models.

Assumption (A2). The function F is strictly convex.

DEFINITION 1.1 (convex neuron model). *We consider the two-dimensional model defined by the equations*

$$(1.1) \quad \begin{cases} \frac{dv}{dt} = F(v) - w + I, \\ \frac{dw}{dt} = a(bv - w), \end{cases}$$

where F satisfies Assumptions (A1) and (A2) and characterizes the passive properties of the membrane potential.

Many neurons of this class blow up in finite time. These neurons are the ones we are interested in.

REMARK. *Note that all the neurons of this class do not blow up in finite time. For instance if $F(v) = v \log(v)$, it will not. For F functions such that $F(v) = (v^{1+\alpha})R(v)$ for some $\alpha > 0$, where $\lim_{v \rightarrow \infty} R(v) > 0$ (possibly ∞), the dynamical system will possibly blow up in finite time.*

If the solution blows up at time t^* , a spike is emitted, and subsequently we have the following reset process:

$$(1.2) \quad \begin{cases} v(t^*) = v_r, \\ w(t^*) = w(t^{*-}) + d, \end{cases}$$

where v_r is the reset membrane potential and $d > 0$ a real parameter. Equations (1.1) and (1.2), together with initial conditions (v_0, w_0) , give us the existence and uniqueness of a solution on \mathbb{R}^+ .

The two parameters v_r and d are important to understand the repetitive spiking properties of the system. Nevertheless, the bifurcation study with respect to these

¹The same study can be done for a parameter-dependent function. More precisely, let $E \subset \mathbb{R}^n$ be a parameter space (for a given n) and $F : E \times \mathbb{R} \rightarrow \mathbb{R}$ a parameter-dependent real function. All the properties shown in this section are valid for any fixed value of the parameter p . Further p -bifurcations studies can be done for specific $F(p, \cdot)$. The first equation can be derived from the general I - V relation in neuronal models: $C \frac{dV}{dt} = I - I_0(V) - g(V - E_K)$, where $I_0(V)$ is the instantaneous I - V curve.

²See, for instance, section 2.2, where the parameters of the initial equation (2.2) are related to biological constants and where we proceed to a dimensionless reduction.

parameters is outside the scope of this paper, and we focus here on the bifurcations of the system with respect to (a, b, I) , in order to characterize the subthreshold behavior of the neuron.

1.2. Fixed points of the system. To understand the qualitative behavior of the dynamical system defined by (1.1) before the blow up (i.e., between two spikes), we begin by studying the fixed points and analyze their stability. The linear stability of a fixed point is governed by the Jacobian matrix of the system, which we define in the following proposition.

PROPOSITION 1.2. *The Jacobian of the dynamical system (1.1) can be written*

$$(1.3) \quad L := v \mapsto \begin{pmatrix} F'(v) & -1 \\ ab & -a \end{pmatrix}.$$

The fixed points of the system satisfy the equations

$$(1.4) \quad \begin{cases} F(v) - bv + I = 0, \\ bv = w. \end{cases}$$

Let $G_b(v) := F(v) - bv$. From (A1) and (A2), we know that the function G_b is strictly convex and has the same regularity as F . To have the same behavior as the IBG models, we want the system to have the same number of fixed points. To this purpose, it is necessary that G_b has a minimum for all $b > 0$. Otherwise, the *convex* function G_b would have no more than one fixed point, since a fixed point of the system is the intersection of an horizontal curve and G_b .

This means for the function F that $\inf_{x \in \mathbb{R}} F'(x) \leq 0$ and $\sup_{x \in \mathbb{R}} F'(x) = +\infty$. Using the monotony property of F' , we write Assumption (A3).

Assumption (A3).

$$\begin{cases} \lim_{x \rightarrow -\infty} F'(x) \leq 0, \\ \lim_{x \rightarrow +\infty} F'(x) = +\infty. \end{cases}$$

Assumptions (A1), (A2), and (A3) ensure us that for all $b \in \mathbb{R}_+^*$, G_b has a unique minimum, denoted $m(b)$, which is reached. Let $v^*(b)$ be the point where this minimum is reached.

This point is the solution of the equation

$$(1.5) \quad F'(v^*(b)) = b.$$

PROPOSITION 1.3. *The point $v^*(b)$ and the value $m(b)$ are continuously differentiable with respect to b .*

Proof. We know that F' is a bijection. The point $v^*(b)$ is defined implicitly by the equation $H(b, v) = 0$, where $H(b, v) = F'(v) - b$. H is a C^1 -diffeomorphism with respect to b , and the differential with respect to b never vanishes. The implicit function theorem (see, for instance, [7, Annex C.6]) ensures us that $v^*(b)$ solution of $H(b, v^*(b)) = 0$ is continuously differentiable with respect to b , and so does $m(b) = G(v^*(b)) - bv^*(b)$. \square

THEOREM 1.4. *The parameter curve defined by $\{(I, b); I = -m(b)\}$ separates three behaviors of the system (see Figure 1.1):*

- (i) *If $I > -m(b)$, then the system has no fixed point.*

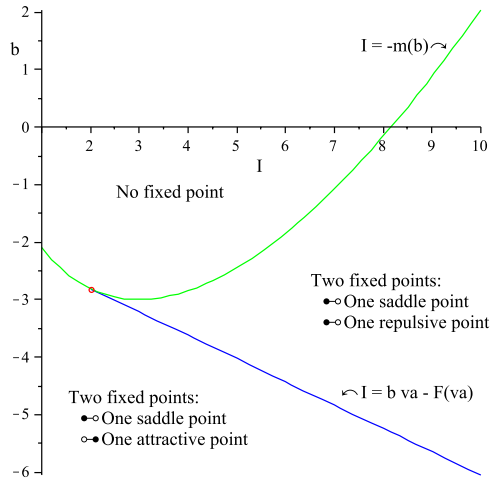


FIG. 1.1. Number of fixed points and their stability in the plane (I, b) for the exponential adaptive model.

- (ii) If $I = -m(b)$, then the system has a unique fixed point, $(v^*(b), w^*(b))$, which is nonhyperbolic. It is unstable if $b > a$.
- (iii) If $I < -m(b)$, then the dynamical system has two fixed points $(v_-(I, b), v_+(I, b))$ such that

$$v_-(I, b) < v^*(b) < v_+(I, b).$$

The fixed point $v_+(I, b)$ is a saddle fixed point, and the stability of the fixed point $v_-(I, b)$ depends on I and on the sign of $(b - a)$:

- (a) If $b < a$, the fixed point $v_-(I, b)$ is attractive.
- (b) If $b > a$, there is a unique smooth curve $I^*(a, b)$ defined by the implicit equation $F'(v_-(I^*(a, b), b)) = a$. This curve reads $I^*(a, b) = b v_a - F(v_a)$, where v_a is the unique solution of $F'(v_a) = a$.
 - (b.1) If $I < I^*(a, b)$, the fixed point is attractive.
 - (b.2) If $I > I^*(a, b)$, the fixed point is repulsive.

Proof.

- (i) We have $F(v) - bv \geq m(b)$ by definition of $m(b)$. If $I > -m(b)$, then for all $v \in \mathbb{R}$ we have $F(v) - bv + I > 0$ and the system has no fixed point.
- (ii) Let $I = -m(b)$. We have already seen that G_b is strictly convex and continuously differentiable and for $b > 0$ reaches its unique minimum at the point $v^*(b)$. This point is such that $G_b(v^*(b)) = m(b)$, and so it is the only point satisfying $F(v^*(b)) - b v^*(b) - m(b) = 0$. Furthermore, this point satisfies $F'(v^*(b)) = b$. The Jacobian of the system at this point reads

$$L(v^*(b)) = \begin{pmatrix} b & -1 \\ ab & -a \end{pmatrix}.$$

Its determinant is 0, and so the fixed point is nonhyperbolic (0 is eigenvalue of the Jacobian matrix). The trace of this matrix is $b - a$. So the fixed point $v^*(b)$ is attractive when $b > a$ and repulsive when $b < a$. The case $a = b$,

$I = -m(b)$ is a degenerate case which we will study more precisely in section 1.3.3.

- (iii) Let $I < -m(b)$. By the strict convexity assumption, Assumption (A2), of the function G together with Assumption (A3), we know that there are only two intersections of the curve G to a level $-I$ higher than its minimum. These two intersections define our two fixed points. At the point v^* the function is strictly lower than $-I$, and so the two solutions satisfy $v_-(I, b) < v^*(b) < v_+(I, b)$.

Let us now study the stability of these two fixed points. To this end, we have to characterize the eigenvalues of the Jacobian matrix of the system at these points.

We can see from formula (1.3) and the convexity assumption, Assumption (A2), that the Jacobian determinant, equal to $-aF'(v) + ab$, is a decreasing function of v and vanishes at $v^*(b)$, and so $\det(L(v_+(I, b))) < 0$ and the fixed point is a saddle point (the Jacobian matrix has a positive and a negative eigenvalue).

For the other fixed point $v_-(I, b)$, the determinant of the Jacobian matrix is strictly positive. So the stability of the fixed point depends on the trace of the Jacobian. This trace reads $F'(v_-(I, b)) - a$.

- (a) When $b < a$, we have a stable fixed point. Indeed, the function F' is an increasing function equal to b at $v^*(b)$, and so $\text{Trace}(L(v_-(I, b))) \leq F'(v^*(b)) - a = b - a < 0$ and the fixed point is attractive.
- (b) If $b > a$, then the type of dynamics around the fixed point v_- depends on the input current (parameter I). Indeed, the trace reads

$$T(I, b, a) := F'(v_-(I, b)) - a,$$

which is continuous and continuously differentiable with respect to I and b , and which is defined for $I < -m(b)$. We have

$$\begin{cases} \lim_{I \rightarrow -m(b)} T(I, b, a) = b - a > 0, \\ \lim_{I \rightarrow -\infty} T(I, b, a) = \lim_{x \rightarrow -\infty} F'(x) - a < 0. \end{cases}$$

So there exists a curve $I^*(a, b)$ defined by $T(I, b, a) = 0$ and such that

- for $I^*(b) < I < -m(b)$, the fixed point $v_-(I, b)$ is repulsive;
- for $I < I^*(b)$, the fixed point v_- is attractive.

To compute the equation of this curve, we use the fact that point $v_-(I^*(b), b)$ is such that $F'(v_-(I^*(b), b)) = a$. We know from the properties of F that there is a unique point v_a satisfying this equation. Since $F'(v^*(b)) = b$, $a < b$, and F' is increasing, the condition $a < b$ implies that $v_a < v^*(b)$.

The associated input current satisfies fixed points equation $F(v_a) - bv_a + I^*(a, b) = 0$, or equivalently

$$I^*(a, b) = bv_a - F(v_a).$$

The point $I = I^*(a, b)$ will be studied in detail in the next section, since it is a bifurcation point of the system. \square

Figure 1.1 represents the different zones enumerated in Theorem 1.4 and their stability in the parameter plane (I, b) .

REMARK. *In this proof, we used the fact that F' is invertible on $[0, \infty)$. Assumption (A3) ensures us that it will be the case and that F has a unique minimum. Assumption (A3) is the weakest possible to have this property.*

1.3. Bifurcations of the system. In the study of the fixed points and their stability, we identified two bifurcation curves where the stability of the fixed points changes. The first curve $I = -m(b)$ corresponds to a saddle-node bifurcation and the curve $I = I^*(a, b)$ to an Andronov–Hopf bifurcation. These two curves meet in a specific point, $b = a$ and $I = -m(a)$. This point has a double 0 eigenvalue, and we show that it is a Bogdanov–Takens bifurcation point.

Let us show that the system undergoes these bifurcations with no other assumption than (A1), (A2), and (A3) on F . We also prove that the system can undergo only one other codimension two bifurcation, a Bautin bifurcation.

1.3.1. Saddle-node bifurcation curve. In this section we characterize the behavior of the dynamical system along the curve of equation $I = -m(b)$, and we prove the following theorem.

THEOREM 1.5. *The dynamical system (1.1) undergoes a saddle-node bifurcation along the parameter curve:*

$$(1.6) \quad (SN) : \{(b, I) ; I = -m(b)\},$$

when $F''(v^*(b)) \neq 0$.

Proof. We derive the normal form of the system at this bifurcation point. Following the works of Guckenheimer and Holmes [9] and Kuznetsov [19], we check only the transversality conditions to be sure that the normal form at the bifurcation point will have the expected form.

Let $b \in \mathbb{R}^+$ and $I = -m(b)$. Let $v^*(b)$ be the unique fixed point of the system for these parameters. The point $v^*(b)$ is the unique solution of $F'(v^*(b)) = b$. At this point, the Jacobian matrix (1.3) reads

$$L(v^*(b)) = \begin{pmatrix} b & -1 \\ ab & -a \end{pmatrix}.$$

This matrix has two eigenvalues 0 and $b - a$. The pairs of right eigenvalues and right eigenvectors are

$$0, U := \begin{pmatrix} 1/b \\ 1 \end{pmatrix} \quad \text{and} \quad b - a, \begin{pmatrix} 1/a \\ 1 \end{pmatrix}.$$

Its pairs of left eigenvalues and left eigenvectors are

$$0, V := (-a, 1) \quad \text{and} \quad b - a, (-b, 1).$$

Let $f_{b,I}$ be the vector field

$$f_{b,I}(v, w) = \begin{pmatrix} F(v) - w + I \\ a(bv - w) \end{pmatrix}.$$

The vector field satisfies

$$\begin{aligned} V \left(\frac{\partial}{\partial I} f_{b,I}(v^*(b), w^*(b)) \right) &= (-a, 1) \cdot \begin{pmatrix} 1 \\ 0 \end{pmatrix} \\ &= -a < 0. \end{aligned}$$

So the coefficient of the normal form corresponding to the Taylor expansion along the parameter I does not vanish.

Finally, let us show that the quadratic terms of the Taylor expansion in the normal form does not vanish. With our notations, this condition reads

$$V\left(D_x^2 f_{b,-m(b)}(v^*(b), w^*(b))(U, U)\right) \neq 0.$$

This property is satisfied in our framework. Indeed,

$$\begin{aligned} V\left(D_x^2 f_{b,-m(b)}(v^*(b), w^*(b))(U, U)\right) &= V\left(\begin{pmatrix} U_1^2 \frac{\partial^2 f_1}{\partial v^2} + 2U_1 U_2 \frac{\partial^2 f_1}{\partial v \partial w} + U_2^2 \frac{\partial^2 f_1}{\partial w^2} \\ U_1^2 \frac{\partial^2 f_2}{\partial v^2} + 2U_1 U_2 \frac{\partial^2 f_2}{\partial v \partial w} + U_2^2 \frac{\partial^2 f_2}{\partial w^2} \end{pmatrix}\right) \\ &= V\left(\begin{pmatrix} \frac{1}{b^2} F''(v^*) \\ 0 \end{pmatrix}\right) \\ &= (-a, 1) \cdot \begin{pmatrix} \frac{1}{b^2} F''(v^*) \\ 0 \end{pmatrix} \\ &= -\frac{a}{b^2} F''(v^*) < 0. \end{aligned}$$

So the system undergoes a saddle-node bifurcation along the manifold $I = -m(b)$. \square

REMARK. Note that $F''(v^*(b))$ can vanish only countably many times since F is strictly convex.

1.3.2. Andronov–Hopf bifurcation curve. In this section we consider the behavior of the dynamical system along the parameter curve $I = I^*(b)$, and we consider the fixed point v_- .

THEOREM 1.6. Let $b > a$, v_a be the unique point such that $F'(v_a) = a$ and $A(a, b)$ be defined by the formula

$$(1.7) \quad A(a, b) := F'''(v_a) + \frac{1}{b-a} (F''(v_a))^2.$$

If $F''(v_a) \neq 0$ and $A(a, b) \neq 0$, then the system undergoes an Andronov–Hopf bifurcation at the point v_a , along the parameter line

$$(1.8) \quad (AH) := \left\{ (b, I) ; b > a \text{ and } I = bv_a - F(v_a) \right\}.$$

This bifurcation is subcritical if $A(a, b) > 0$ and supercritical if $A(a, b) < 0$.

Proof. The Jacobian matrix at the point v_a reads

$$L(v_a) = \begin{pmatrix} a & -1 \\ ab & -a \end{pmatrix}.$$

Its trace is 0 and its determinant is $a(b-a) > 0$, and so the matrix at this point has a pair of pure imaginary eigenvalues $(i\omega, -i\omega)$, where $\omega = \sqrt{a(b-a)}$. Along the curve of equilibria when I varies, the eigenvalues are complex conjugates with real part $\mu(I) = \frac{1}{2} \text{Tr}(L(v_-(I, b)))$ which vanishes at $I = I^*(a, b)$.

We recall that from Proposition 1.3, this trace varies smoothly with I . Indeed, $v_-(b, I)$ satisfies $F(v_-(I, b)) - bv_-(I, b) + I = 0$ and is differentiable with respect to I . We have

$$\frac{\partial v_-(I, b)}{\partial I} (F'(v_-(I, b)) - b) = -1.$$

At the point $v_-(I^*(b), b) = v_a$, we have $F'(v_a) = a < b$, and so for I close to this equilibrium point, we have

$$\frac{\partial v_-(I, b)}{\partial I} > 0.$$

Now let us check that the transversality condition of an Andronov–Hopf bifurcation is satisfied (see [9, Theorem 3.4.2]). There are two conditions to be satisfied: the transversality condition $\frac{d\mu(I)}{dI} \neq 0$ and the nondegeneracy condition $l_1 \neq 0$, where l_1 is the first Lyapunov coefficient at the bifurcation point.

First of all, we prove that the transversality condition is satisfied:

$$\begin{aligned} \mu(I) &= \frac{1}{2} \text{Tr}(L(v_-(I, b))) \\ &= \frac{1}{2} (F'(v_-(I, b)) - a), \\ \frac{d\mu(I)}{dI} &= \frac{1}{2} F''(v_-(I, b)) \frac{dv_-(I, b)}{dI} \\ &> 0. \end{aligned}$$

Let us now write the normal form at this point. To this purpose, we change variables:

$$\begin{cases} v - v_a = x, \\ w - w_a = ax + \omega y. \end{cases}$$

The (x, y) equation reads

$$(1.9) \quad \begin{cases} \dot{x} = -\omega y + (F(x + v_a) - ax - w_a) =: -\omega y + f(x), \\ \dot{y} = \omega x + \frac{a}{\omega}(ax - F(x + v_a) + w_a - I) =: \omega x + g(x). \end{cases}$$

According to Guckenheimer in [9], we state that the Lyapunov coefficient of the system at this point has the same sign as B , where B is defined by

$$B := \frac{1}{16} [f_{xxx} + f_{xyy} + g_{xxy} + g_{yyx}] + \frac{1}{16\omega} [f_{xy}(f_{xx} + f_{yy}) - g_{xy}(g_{xx} + g_{yy}) - f_{xx}g_{xx} + f_{yy}g_{yy}].$$

Replacing f and g by the expressions found in (1.9), we obtain the expression of A :

$$\begin{aligned} B &= \frac{1}{16} F'''(v_a) + \frac{a}{16\omega^2} (F''(v_a))^2 \\ &= \frac{1}{16} F'''(v_a) + \frac{1}{16(b-a)} (F''(v_a))^2 \\ &= \frac{1}{16} A(a, b). \end{aligned}$$

Hence when $A(a, b) \neq 0$, the system undergoes an Andronov–Hopf bifurcation. When $A(a, b) > 0$, the bifurcation is subcritical and the periodic orbits generated by the Hopf bifurcation are repelling, and when $A(a, b) < 0$, the bifurcation is supercritical and the periodic orbits are attractive (the formula of A has also been introduced by Izhikevich in [16, eq. (15), p. 213]). \square

REMARK. The case $A(a, b) = 0$ is not treated in the theorem and is a little bit more intricate. We fully treat it in section 1.3.4 and show that a Bautin (generalized Hopf) bifurcation can occur if the A -coefficient vanishes. Since the third derivative is a priori unconstrained, this case can occur, and we prove in section 3 that this is the case for a simple (quartic) model.

1.3.3. Bogdanov–Takens bifurcation. We have seen in the study that this formal model presents an interesting point in the parameter space, corresponding to the intersection of the saddle-node bifurcation curve and the Andronov–Hopf bifurcation curve. At this point, we show that the system undergoes a Bogdanov–Takens bifurcation.

THEOREM 1.7. Let F be a real function satisfying Assumptions (A1), (A2), and (A3). Let $a \in \mathbb{R}_+^*$ and $b = a$, and let v_a be the only point such that $F'(v_a) = a$. Assume again that $F''(v_a) \neq 0$.

Then at this point and with these parameters, the dynamical system (1.1) undergoes a subcritical Bogdanov–Takens bifurcation of normal form:

$$(1.10) \quad \begin{cases} \dot{\eta}_1 = \eta_2, \\ \dot{\eta}_2 = \left(\frac{8F''(v_a)aI_1}{(a+b_1)^3} \right) - \left(\frac{2(2b_1 a + I_1 F''(v_a))}{(a+b_1)^2} \right) \eta_1 + \eta_1^2 + \eta_1 \eta_2 + \mathcal{O}(\|\eta\|^3), \end{cases}$$

where $b_1 := b - a$ and $I_1 = I + m(a)$.

Proof. The Jacobian matrix (1.3) at this point reads

$$L(v_a) = \begin{pmatrix} a & -1 \\ a^2 & -a \end{pmatrix}.$$

This matrix is nonzero and has two 0 eigenvalues (its determinant and trace are 0). The matrix $Q := \begin{pmatrix} a & 1 \\ a^2 & -a \end{pmatrix}$ is the passage matrix to the Jordan form of the Jacobian matrix:

$$Q^{-1} \cdot L(v_a) \cdot Q = \begin{pmatrix} 0 & 1 \\ 0 & 0 \end{pmatrix}.$$

To prove that the system undergoes a Bogdanov–Takens bifurcation, we show that the normal form reads

$$(1.11) \quad \begin{cases} \dot{\eta}_1 = \eta_2, \\ \dot{\eta}_2 = \beta_1 + \beta_2 \eta_1 + \eta_1^2 + \sigma \eta_1 \eta_2 + \mathcal{O}(\|\eta\|^3) \end{cases}$$

with $\sigma = \pm 1$. The proof of this theorem consists of (i) proving that the system undergoes a Bogdanov–Takens bifurcation, (ii) finding a closed-form expression for the variables β_1 and β_2 , and (iii) proving that $\sigma = 1$.

First of all, let us prove that the normal form can be written in the form of (1.11). This is equivalent to showing some transversality conditions on the system (see, for instance, [19, Theorem 8.4]).

To this end, we center the equation at this point and write the system in the coordinates given by the Jordan form of the matrix. Let $\begin{pmatrix} y_1 \\ y_2 \end{pmatrix} = Q^{-1} \begin{pmatrix} v - v_a \\ w - w_a \end{pmatrix}$ at the point $b = a + b_1$, $I = -m(a) + I_1$. We get

$$(1.12) \quad \begin{cases} \dot{y}_1 = y_2 + \frac{b_1}{a}(ay_1 + y_2), \\ \dot{y}_2 = F(ay_1 + y_2 + v_a) - w_a - m(a) + I_1 - a^2 y_1 - ay_2 - b_1(ay_1 + y_2). \end{cases}$$

Let us denote $v_1 = ay_1 + y_2$. The Taylor expansion on the second equation gives us

$$\begin{aligned}
 \dot{y}_2 &= F(v_1 + v_a) - w_a - m(a) + I_1 - a^2y_1 - ay_2 - b_1(ay_1 + y_2) \\
 &= F(v_a) + F'(v_a)v_1 + \frac{1}{2}F''(v_a)v_1^2 - w_a - m(a) \\
 &\quad + I_1 - a^2y_1 - ay_2 - b_1(ay_1 + y_2) + \mathcal{O}(\|v_1\|^3) \\
 &= (F(v_a) - w_a - m(a)) + I_1 + (F'(v_a) - a)v_1 - b_1v_1 + \frac{1}{2}F''(v_a)v_1^2 \\
 &\quad + \mathcal{O}(\|v_1\|^3) \\
 (1.13) \quad &= I_1 - b_1(ay_1 + y_2) + \frac{1}{2}F''(v_a)(ay_1 + y_2)^2 + \mathcal{O}(\|y\|^3).
 \end{aligned}$$

Let us denote for the sake of clarity $\alpha = (b_1, I_1)$ and write (1.12) as

$$(1.14) \quad \begin{cases} \dot{y}_1 = y_2 + a_{00}(\alpha) + a_{10}(\alpha)y_1 + a_{01}(\alpha)y_2, \\ \dot{y}_2 = b_{00}(\alpha) + b_{10}(\alpha)y_1 + b_{01}(\alpha)y_2 + \frac{1}{2}b_{20}(\alpha)y_1^2 + b_{11}(\alpha)y_1y_2 + \frac{1}{2}b_{02}(\alpha)y_2^2 + \mathcal{O}(\|y\|^3). \end{cases}$$

From (1.12) and (1.13), it is straightforward to identify the expressions for the coefficients $a_{ij}(\alpha)$ and $b_{ij}(\alpha)$.

Let us now use the change of variables:

$$\begin{cases} u_1 = y_1, \\ u_2 = y_2 + \frac{b_1}{a}(ay_1 + y_2). \end{cases}$$

The dynamical system governing (u_1, u_2) reads

$$\begin{cases} \dot{u}_1 = u_2, \\ \dot{u}_2 = (1 + \frac{b_1}{a}) - b_1 a u_1 + \frac{1}{2} \frac{a^3 F''(v_a)}{a+b_1} u_1^2 + \frac{a^2 F''(v_a)}{a+b_1} u_1 u_2 + \frac{1}{2} \frac{a F''(v_a)}{a+b_1} u_2^2. \end{cases}$$

The transversality conditions of a Bogdanov–Takens bifurcation [9, 19] can easily be verified from this expression:

- (BT.1) The Jacobian matrix is not 0.
- (BT.2) With the notations of (1.14), we have $a_{20} = 0$ and $b_{11}(0) = aF''(v_a) > 0$, and so $a_{20}(0) + b_{11}(0) = aF''(v_a) > 0$.
- (BT.3) $b_{20} = a^2F''(v_a) > 0$.
- (BT.4) We show that the map

$$\left(x := \begin{pmatrix} y_1 \\ y_2 \end{pmatrix}, \alpha := \begin{pmatrix} I_1 \\ b_1 \end{pmatrix} \right) \mapsto \left[f(x, \alpha), \text{Tr}(D_x f(x, \alpha)), \text{Det}(D_x f(x, \alpha)) \right]$$

is regular at the point of interest.

From the two first assumptions, we know that the system can be put in the form of (1.11). Guckenheimer in [9] proves that this condition can be reduced to the nondegeneracy of the differential with respect to (I_1, b_1) of the vector $\begin{pmatrix} \beta_1 \\ \beta_2 \end{pmatrix}$ of (1.11).

In our case, we can compute these variables β_1 and β_2 following the calculation steps of [19], and we get

$$(1.15) \quad \begin{cases} \beta_1 = \frac{8F''(v_a)aI_1}{(a+b_1)^3}, \\ \beta_2 = -\frac{2(2b_1a+I_1)F''(v_a)}{(a+b_1)^2}. \end{cases}$$

Hence the differential of the vector $\begin{pmatrix} \beta_1 \\ \beta_2 \end{pmatrix}$ with respect to the parameters (I_1, b_1) at the point $(0, 0)$ reads

$$D_\alpha \beta|_{(0,0)} = \begin{pmatrix} \frac{8F''(v_a)}{a^2} & 0 \\ -2\frac{F''(v_a)}{a^2} & -4/a \end{pmatrix}.$$

This matrix has a nonzero determinant if and only if $F''(v_a) \neq 0$.

Therefore we have proved the existence of a Bogdanov–Takens bifurcation under the condition $F''(v_a) \neq 0$.

Let us now show that $\sigma = 1$. Indeed, this coefficient is given by the sign of $b_{20}(0)(a_{20}(0) + b_{11}(0))$ which in our case is equal to $a^3 F''(v_a)^2 > 0$, and so the bifurcation is always of the type (1.10) (generation of an unstable limit cycle) for all the members of our class of models. \square

The existence of a Bogdanov–Takens bifurcation point implies the existence of a smooth curve corresponding to a saddle homoclinic bifurcation in the system (see [19, Lemma 8.7]).

COROLLARY 1.8. *There is a unique smooth curve (P) corresponding to a saddle homoclinic bifurcation in the system (1.1) originating at the parameter point $b = a$ and $I = -m(a)$ defined by the implicit equation:*

$$(1.16) \quad (P) := \left\{ \begin{aligned} & (I = -m(a) + I_1, b = a + b_1) ; \\ & I_1 = \frac{\left(-\frac{25}{6}a - \frac{37}{6}b_1 + \frac{5}{6}\sqrt{25a^2 + 74b_1a + 49b_1^2}\right)a}{F''(v_a)} + o(|b_1| + |I_1|) \\ & \text{and } b_1 > -\frac{I_1 F''(v_a)}{2a} \end{aligned} \right\}.$$

Moreover, for (b, I) in a neighborhood of $(a, -m(a))$, the system has a unique and hyperbolic unstable cycle for parameter values inside the region bounded by the Hopf bifurcation curve and the homoclinic bifurcation curve (P) , and it has no cycle outside this region.

Proof. As noticed, from the Bogdanov–Takens bifurcation point, we have the existence of this saddle homoclinic bifurcation curve. Let us now compute the equation of this curve in the neighborhood of the Bogdanov–Takens point. To this purpose we use the normal form we derived in Theorem 1.7 and use the local characterization given, for instance, in [19, Lemma 8.7] for the saddle homoclinic curve:

$$(P) := \left\{ (\beta_1, \beta_2) ; \beta_1 = -\frac{6}{25}\beta_2^2 + o(\beta_2^2), \beta_2 < 0 \right\}.$$

Using the expressions (1.15) yields

$$(P) := \left\{ \begin{aligned} & (I = -m(a) + I_1, b = a + b_1) ; \\ & \frac{8F''(v_a)aI_1}{(a + b_1)^3} = \frac{24(2b_1a + I_1F''(v_a))^2}{25(a + b_1)^4} + o(|b_1| + |I_1|) \\ & \text{and } b_1 > -\frac{I_1 F''(v_a)}{2a} \end{aligned} \right\}.$$

We can solve this equation. There are two solutions but only one satisfying $I_1 = 0$ when $b_1 = 0$. This solution is the curve of saddle homoclinic bifurcations. \square

1.3.4. Formal conditions for a Bautin bifurcation. In the study of the Andronov–Hopf bifurcation, we showed that the sub- or supercritical type of bifurcation depended on the variable $A(a, b)$ defined by (1.7). If this variable changes sign when b varies, then the stability of the limit cycle along Hopf bifurcation changes stability. This can occur if the point v_a satisfies the following condition.

Assumption (A4). For v_a such that $F'(v_a) = a$, we have

$$F'''(v_a) < 0.$$

Indeed, if this happens, the type of Andronov–Hopf bifurcation changes, since we have

$$\begin{cases} \lim_{b \rightarrow a^-} A(a, b) = +\infty, \\ \lim_{b \rightarrow +\infty} A(a, b) = F'''(v_a) < 0. \end{cases}$$

In this case the first Lyapunov exponent vanishes for

$$b = a - \frac{(F''(v_a))^2}{F'''(v_a)}.$$

At this point, the system has the characteristics of a Bautin (generalized Hopf) bifurcation. Nevertheless, we still have to check two nondegeneracy conditions to ensure that the system actually undergoes a Bautin bifurcation:

(BGH.1) The second Lyapunov coefficient of the dynamical system l_2 does not vanish at this equilibrium point.

(BGH.2) Let $l_1(I, b)$ be the first Lyapunov exponent of this system and $\mu(I, b)$ the real part of the eigenvalues of the Jacobian matrix. The map

$$(I, b) \mapsto (\mu(I, b), l_1(I, b))$$

is regular at this point.

In this case the system would be locally topologically equivalent to the normal form:

$$\begin{cases} \dot{y}_1 = \beta_1 y_1 - y_2 + \beta_2 y_1 (y_1^2 + y_2^2) + \sigma y_1 (y_1^2 + y_2^2)^2, \\ \dot{y}_2 = \beta_1 y_2 - y_1 + \beta_2 y_2 (y_1^2 + y_2^2) + \sigma y_2 (y_1^2 + y_2^2)^2. \end{cases}$$

We reduce the problem to the point that checking the two conditions of a BGH bifurcation becomes straightforward.

Let (v_a, w_a) be the point where the system undergoes the Bautin bifurcation (when it exists). Since we already computed the eigenvalues and eigenvectors of the Jacobian matrix along the Andronov–Hopf bifurcation curve, we can use it to reduce the problem. The basis where we express the system is given by

$$\begin{cases} Q := \begin{pmatrix} \frac{1}{b} & \frac{\omega}{ab} \\ 1 & 0 \end{pmatrix}, \\ \begin{pmatrix} x \\ y \end{pmatrix} := Q^{-1} \begin{pmatrix} v - v_a \\ w - w_a \end{pmatrix}. \end{cases}$$

Let us write the dynamical equations satisfied by (x, y) :

$$\begin{cases} \dot{x} = \omega y, \\ \dot{y} = \frac{ab}{\omega} \left(F\left(v_a + \frac{1}{b}x + \frac{\omega}{ab}y\right) - w_a - x + I_a - ay \right). \end{cases}$$

To ensure that we have a Bautin bifurcation at this point we will need to perform a Taylor expansion up to the fifth order, and so we need to make the following assumption.

Assumption (A5). The function F is six times continuously differentiable at (v_a, w_a) .

First, let us denote $v_1(x, y) = \frac{1}{b}x + \frac{\omega}{ab}y$; the Taylor expansion reads

$$\begin{aligned} \dot{y} &= \frac{ab}{\omega} \left(F(v_a) - w_a + I \right) + \frac{ab}{\omega} \left[F'(v_a)v_1(x, y) - ay \right] + \frac{1}{2} \frac{ab}{\omega} \left[F''(v_a)v_1(x, y)^2 \right] \\ &+ \frac{1}{6} \frac{ab}{\omega} F'''(v_a)v_1(x, y)^3 + \frac{1}{4!} \frac{ab}{\omega} F^{(4)}(v_a)v_1(x, y)^4 \\ &+ \frac{1}{5!} \frac{ab}{\omega} F^{(5)}(v_a)v_1(x, y)^5 + \mathcal{O} \left(\left\| \begin{pmatrix} x \\ y \end{pmatrix} \right\|^6 \right). \end{aligned}$$

This expression, together with the complex left and right eigenvectors of the Jacobian matrix, allows us to compute the first and second Lyapunov coefficients and to check the existence of a Bautin bifurcation.

Nevertheless, we cannot push the computation any further at this level of generality, but, for a given function F presenting a change in the sign of $A(a, b)$, this can easily be done through the use of a symbolic computation package. The interested reader is referred to Appendix A for checking the Bautin bifurcation transversality conditions, where calculations are given for the quartic neuron model.

1.4. Conclusion: The full bifurcation diagram. We now summarize the results obtained in this section in the two following theorems.

THEOREM 1.9. *Let us consider the formal dynamical system*

$$(1.17) \quad \begin{cases} \dot{v} = F(v) - w + I, \\ \dot{w} = a(bv - w), \end{cases}$$

where a is a fixed real, b and I bifurcation parameters, and $F : \mathbb{R} \mapsto \mathbb{R}$ a real function. If the function F satisfies the assumptions that

- (A.1) the function F is three times continuously differentiable,
- (A.2) F is strictly convex, and
- (A.3) F' satisfies the conditions

$$\begin{cases} \lim_{x \rightarrow -\infty} F'(x) \leq 0, \\ \lim_{x \rightarrow \infty} F'(x) = \infty, \end{cases}$$

then the dynamical system (1.17) shows the following bifurcations:

(B1) A saddle-node bifurcation curve:

$$(SN) : \{(b, I) ; I = -m(b)\},$$

where $m(b)$ is the minimum of the function $F(v) - bv$ (if the second derivative of F does not vanish at this point).

(B2) An Andronov–Hopf bifurcation line:

$$(AH) := \left\{ (b, I) ; b > a \text{ and } I = bv_a - F(v_a) \right\},$$

where v_a is the unique solution of $F'(v_a) = a$ (if $F''(v_a) \neq 0$). This type of Andronov–Hopf bifurcation is given by the sign of the variable

$$A(a, b) = F'''(v_a) + \frac{1}{b-a} F''(v_a)^2.$$

If $A(a, b) > 0$, then the bifurcation is subcritical, and if $A(a, b) < 0$, then the bifurcation is supercritical.

(B3) A Bogdanov–Takens bifurcation point at the point $b = a$ and $I = -m(a)$ if $F''(v_a) \neq 0$.

(B4) A saddle homoclinic bifurcation curve characterized in the neighborhood of the Bogdanov–Takens point by

$$(P) := \left\{ \begin{aligned} & (I = -m(a) + I_1, b = a + b_1) ; \\ & I_1 = \frac{\left(-\frac{25}{6} a - \frac{37}{6} b_1 + \frac{5}{6} \sqrt{25 a^2 + 74 b_1 a + 49 b_1^2}\right) a}{F''(v_a)} + o(|b_1| + |I_1|) \\ & \text{and } b_1 > -\frac{I_1 F''(v_a)}{2a} \end{aligned} \right\}.$$

THEOREM 1.10. Consider the system (1.1), where a is a given real number, b and I are real bifurcation parameters, and $F : E \times \mathbb{R} \mapsto \mathbb{R}$ is a function satisfying the following assumptions:

- (A.5) The function F is six times continuously differentiable.
- (A.2) F is strictly convex.
- (A.3) F' satisfies the conditions

$$\begin{cases} \lim_{x \rightarrow -\infty} F'(x) \leq 0, \\ \lim_{x \rightarrow \infty} F'(x) = \infty. \end{cases}$$

(A.4) Let v_a be the unique real such that $F'(v_a) = a$. We have

$$F'''(v_a) < 0.$$

Furthermore, consider the following conditions:

- (BGH.1) The second Lyapunov coefficient of the dynamical system $l_2(v_a) \neq 0$.
- (BGH.2) Let $l_1(v)$ denote the first Lyapunov exponent and $\lambda(I, b) = \mu(I, b) \pm i\omega(I, b)$ the eigenvalues of the Jacobian matrix in the neighborhood of the point of interest. The map $(I, b) \rightarrow (\mu(I, b), l_1(I, b))$ is regular at this point.

Having these, the system undergoes a Bautin bifurcation at the point v_a for the parameters $b = a - \frac{F''(v_a)^2}{F'''(v_a)}$ and $I = bv_a - F(v_a)$.

REMARK. Theorem 1.9 enumerates some of the bifurcations that any dynamical system of the class (1.1) will always undergo. Together with Theorem 1.10, they summarize all the local bifurcations the system can undergo, and no other fixed-point bifurcation is possible. In section 3 we introduce a model actually showing all these local bifurcations.

2. Applications: Izhikevich and Brette–Gerstner models. In this section we show that the neuron models proposed by Izhikevich in [14] and Brette and Gerstner in [5] are part of the class studied in section 1. Using the results of the latter section, we derive their bifurcation diagram and obtain that they show exactly the same types of bifurcations.

2.1. Izhikevich quadratic adaptive model. We produce here a complete description of the bifurcation diagram of the adaptive quadratic integrate-and-fire model proposed by Izhikevich in [14] and [16, Chapter 8]. We use here the dimensionless equivalent version of this model with the fewest parameters:

$$(2.1) \quad \begin{cases} \dot{v} = v^2 - w + I, \\ \dot{w} = a(bv - w). \end{cases}$$

Equation (2.1) is clearly a particular case of (1.1) with

$$F(v) = v^2.$$

F is clearly strictly convex and C^∞ . $F'(v) = 2v$, and so it also satisfies Assumption (A3). Furthermore, the second derivative never vanishes, and so the system undergoes the three bifurcations stated in Theorem 1.9.

(Izh.B1) A saddle-node bifurcation curve defined by

$$\left\{ (b, I) ; I = \frac{b^2}{4} \right\}.$$

For $(I, b) \in \mathbb{R}^2$, the fixed point is given by $(v^*(b) = \frac{1}{2}b, w^*(b) = \frac{1}{2}b^2)$.

For $I < \frac{b^2}{4}$, the fixed point(s) are

$$v_{\pm}(b, I) = \frac{1}{2}(b \pm \sqrt{b^2 - 4I}).$$

(Izh.B2) An Andronov–Hopf bifurcation line:

$$\left\{ (I, b) ; b > a \text{ and } I = \frac{a}{2} \left(b - \frac{a}{2} \right) \right\},$$

whose type is given by the sign of the variable

$$A(a, b) = \frac{4}{b - a}.$$

This value is always strictly positive, and so the bifurcation is always subcritical.

(Izh.B3) A Bogdanov–Takens bifurcation point for $b = a$ and $I = \frac{a^2}{4}$, $v_a = \frac{a}{2}$.

(Izh.B4) A saddle homoclinic bifurcation curve satisfying the quadratic equation near the Bogdanov–Takens point:

$$(P) := \left\{ \left(I = \frac{a^2}{2} + I_1, b = a + b_1 \right) ; \right. \\ \left. I_1 = \frac{a}{2} \left(-\frac{25}{6}a - \frac{37}{6}b_1 + \frac{5}{6} \sqrt{25a^2 + 74b_1a + 49b_1^2} \right) + o(|b_1| + |I_1|) \right. \\ \left. \text{and } b_1 > -\frac{I_1}{a} \right\}.$$

Figure 2.1 represents the fixed points of this dynamical system, and their stability, together with the bifurcation curves.

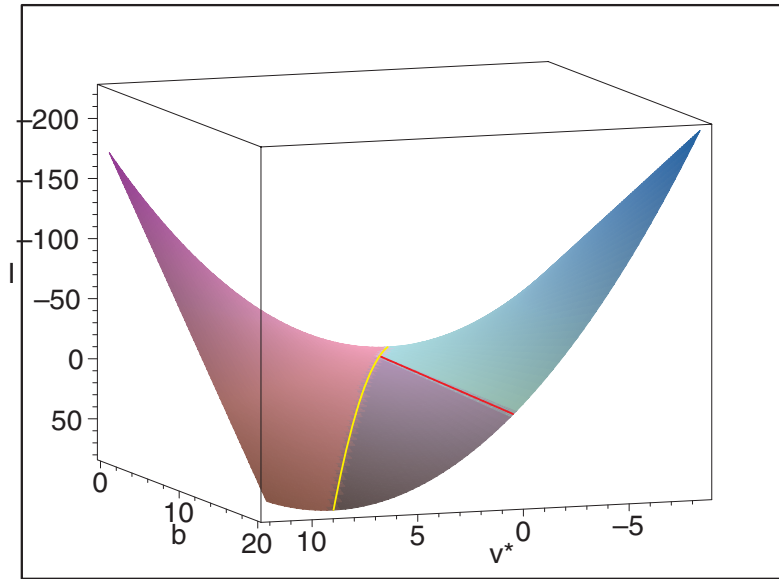


FIG. 2.1. Representation of the v fixed point with respect to the parameters I and b in the Izhikevich model. The reddish component is the surface of saddle fixed points, the purplish one corresponds to the repulsive fixed points, and the greenish/bluish one corresponds to the attractive fixed points. The yellow curve corresponds to a saddle-node bifurcation and the red one to an Andronov–Hopf bifurcation.

2.2. Brette–Gerstner exponential adaptive integrate-and-fire neuron.

In this section we study the bifurcation diagram of the adaptive exponential neuron. This model has been introduced by Brette and Gerstner in [5]. This model, inspired by the Izhikevich adaptive quadratic model, can be fitted to biological values, takes into account the adaptation phenomenon, and is able to reproduce many behaviors observed in cortical neurons. The bifurcation analysis we derived in section 1 allows us to understand how the parameters of the model can affect the behavior of this neuron. We show that this model is part of the general class studied in section 1, and we obtain the fixed-point bifurcation diagram of the model.

2.2.1. Reduction of the original model. This original model is based on biological constants and is expressed with a lot of parameters. We first reduce this model to a simpler form with the fewest number of parameters.

The basic equations proposed in the original paper [5] read

$$(2.2) \quad \begin{cases} C \frac{dV}{dt} = -g_L(V - E_L) + g_L \Delta_T \exp\left(\frac{V - V_T}{\Delta_T}\right) \\ \quad - g_e(t)(V - E_e) - g_i(t)(V - E_i) - W + I_m, \\ \tau_W \frac{dW}{dt} = \kappa(V - E_L) - W. \end{cases}$$

First, we do not assume that the reversal potential of the w equation is the same as the leakage potential E_L , and we write the equation for the adaptation variable by

$$\tau_W \frac{dW}{dt} = a(V - \bar{V}) - W.$$

Next we assume that $g_e(\cdot)$ and $g_i(\cdot)$ are constant (in the original paper it was assumed that the two conductances were null).

After some straightforward algebra, we eventually get the following dimensionless equation equivalent to (2.2):

$$(2.3) \quad \begin{cases} \dot{v} = -v + e^v - w + I, \\ \dot{w} = a(bv - w), \end{cases}$$

where we denoted

$$(2.4) \quad \begin{cases} \tilde{g} := g_L + g_e + g_i, \\ \tau_m := \frac{C}{\tilde{g}}, \\ B := \frac{\kappa}{\tilde{g}} \left(\frac{E_L}{\Delta_T} + \log\left(\frac{g_L}{\tilde{g}} e^{-V_T/\Delta_T}\right) \right), \\ v(\tau) := \frac{V(\tau\tau_m)}{\Delta_T} + \log\left(\frac{g_L}{\tilde{g}} e^{-V_T/\Delta_T}\right), \\ w(\tau) := \frac{W(\tau\tau_m)}{\tilde{g}\Delta_T} + B, \\ a := \frac{\tau_m}{\tau_W}, \\ b := \frac{\kappa}{\tilde{g}}, \\ I := \frac{I_m + g_L E_L + g_e E_e + g_i E_i}{\tilde{g}\Delta_T} + \log\left(\frac{g_L}{\tilde{g}} e^{-V_T/\Delta_T}\right) + B \end{cases}$$

and where the dot denotes the derivative with respect to τ .

REMARK. *These expressions confirm the qualitative interpretation of the parameters a , b , and I of the model (1.1). Indeed, $a = \frac{\tau_m}{\tau_W}$ accounts for the time scale of the adaptation (with the membrane time scale as reference), and the parameter $b = \frac{\kappa}{\tilde{g}}$ is proportional to the interaction between the membrane potential and the adaptation variable and inversely proportional to the total conductivity of the membrane potential. Eventually, I is an affine function of the input current I_m and models the input current of the neurons.*

2.2.2. Bifurcation diagram. From (2.3) we can clearly see that the Brette–Gerstner model is included in the formal class studied in the paper with

$$F(v) = e^v - v.$$

This function satisfies Assumptions (A1), (A2), and (A3). Furthermore, its second order derivative never vanishes.

Theorem 1.9 shows that the system undergoes the following bifurcations:

(BG.B1) A saddle-node bifurcation curve defined by

$$\{(b, I) ; I = (1 + b)(1 - \log(1 + b))\}.$$

So $v^*(b) = \log(1 + b)$. For $I \leq (1 + b)(1 - \log(1 + b))$, the system has the fixed points

$$(2.5) \quad \begin{cases} v_-(I, b) := -W_0\left(-\frac{1}{1+b}e^{\frac{I}{1+b}}\right) + \frac{I}{1+b}, \\ v_+(I, b) := -W_{-1}\left(-\frac{1}{1+b}e^{\frac{I}{1+b}}\right) + \frac{I}{1+b}, \end{cases}$$

where W_0 is the principal branch of Lambert's W function³ and W_{-1} the real branch of Lambert's W function such that $W_{-1}(x) \leq -1$, defined for $-e^{-1} \leq x < 1$.

³The Lambert W function is the inverse function of $x \mapsto xe^x$.

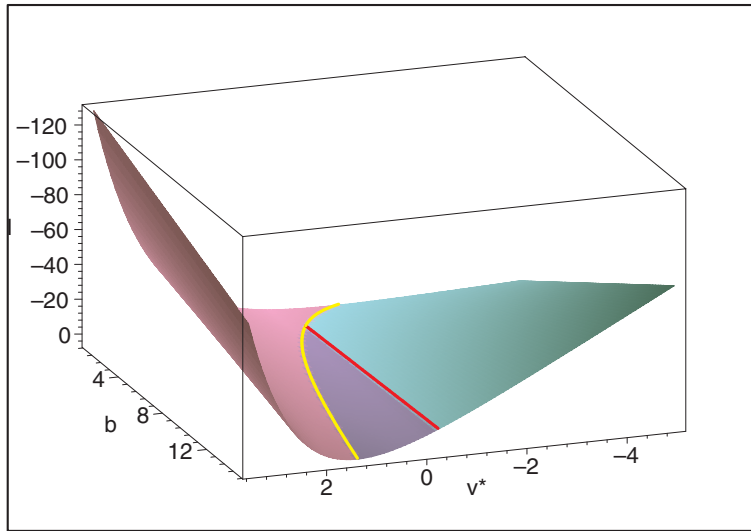


FIG. 2.2. Representation of the v fixed point of the Brette–Gerstner model with respect to the parameters I and b . The reddish/pinkish component is the surface of saddle fixed points, the purplish one corresponds to the repulsive fixed points, and the bluish/greenish one corresponds to the attractive fixed points. The yellow curve corresponds to a saddle–node bifurcation and the red one to an Andronov–Hopf bifurcation.

(BG.B2) An Andronov–Hopf bifurcation line for

$$\{(b, I) ; b > a \text{ and } I = I^*(a, b) = (1 + b) \log(1 + a) - (1 + a)\}$$

at the equilibrium point $(v_a = \log(1 + a), w_a = bv_a)$. This type of Andronov–Hopf bifurcation is given by the sign of the variable

$$A(a, b) = F'''(v_a) + \frac{1}{b - a} F''(v_a)^2 = (1 + a) + \frac{4}{b - a} (1 + a)^2 > 0.$$

So the bifurcation is always subcritical, and there is not any Bautin bifurcation.

(BG.B3) A Bogdanov–Takens bifurcation point at the point $b = a$ and $I = \log(1 + a)$.

(BG.B4) A saddle homoclinic bifurcation curve satisfying, near the Bogdanov–Takens point, the equation

$$(P) := \left\{ \begin{aligned} & (I = (1 + a)(\log(1 + a) - 1) + I_1, b = a + b_1) ; \\ & I_1 = \frac{\left(-\frac{25}{6} a - \frac{37}{6} b_1 + \frac{5}{6} \sqrt{25 a^2 + 74 b_1 a + 49 b_1^2}\right) a}{(1 + a)} + o(|b_1| + |I_1|) \\ & \text{and } b_1 > -\left(1 + \frac{1}{a}\right) I_1 \end{aligned} \right\}.$$

In Figure 2.2 we represent the fixed points of the exponential model and their stability, together with the bifurcation curves, in the space (I, b, v) .

3. The richer quartic model. In this section, we introduce a new specific model having a richer bifurcation diagram than the two models studied in section 2. It is as simple as the two previous models from the mathematical and computational points of view. To this end, we define a model which is part of the class studied in section 1 by specifying the function F .

3.1. The quartic model: Definition and bifurcation map. Let $a > 0$ be a fixed real and $\alpha > a$. We instantiate the model (1.1) with the function F a quartic polynomial:

$$F(v) = v^4 + 2av.$$

REMARK. *The choice of the function F here is just an example where all the formulas are rather simple. Exactly the same analysis can be done with any F function satisfying $F'''(v_a) < 0$ and the transversality conditions given in Theorem 1.10. This would be the case, for instance, for any quartic polynomial $F(v) = v^4 + \alpha v$ for $\alpha > a$.*

The function F satisfies Assumptions (A1), (A2), and (A5). $F'(v) = 4v^3 + 2a$ satisfies Assumption (A3).

Nevertheless, we have to bear in mind that the second order derivative vanishes at $v = 0$:

$$(3.1) \quad \begin{cases} \dot{v} = v^4 + 2av - w + I, \\ \dot{w} = a(bv - w). \end{cases}$$

Theorem 1.9 shows that the quartic model undergoes the following bifurcations:

(B1) A saddle-node bifurcation curve defined by

$$(SN) := \left\{ (b, I) ; I = 3 \left(\frac{b-2a}{4} \right)^{(4/3)} \right\}.$$

Proof. Indeed, the function G reads $G(v) = v^4 + (2a - b)v$ and reaches its minimum at the point $v = \left(\frac{b-2a}{4} \right)^{(1/3)}$. So the minimum of G is $m(b) = -3 \left(\frac{b-2a}{4} \right)^{(4/3)}$. \square

The point $v^*(b)$ is $\left(\frac{b-2a}{4} \right)^{(1/3)}$, and we have closed-form expressions (but rather complicated) for the two fixed points for $I < 3 \left(\frac{b-2a}{4} \right)^{(4/3)}$ since the quartic equation is solvable in radicals. The closed form expression can be obtained using a symbolic computation package like Maple using the command

```
S:=allvalues( solve( x^4 + (2*a - b) * x + I0 = 0, x));
```

(B2) An Andronov–Hopf bifurcation curve for $b > a$ along the straight line

$$(AH) := \left\{ (I, b) ; b > a \text{ and } I = - \left(\frac{a}{4} \right)^{1/3} b - \left(\frac{a}{4} \right)^{4/3} \right\}.$$

The fixed point where the system undergoes this bifurcation is $v_a = -\left(\frac{a}{4} \right)^{1/3}$. The kind of Andronov–Hopf bifurcation we have is governed by the sign of

$$\alpha = -24 \left(\frac{a}{4} \right)^{1/3} + \frac{144}{b-a} \left(\frac{a}{4} \right)^{4/3}.$$

Finally, the type of bifurcation changes when b varies.

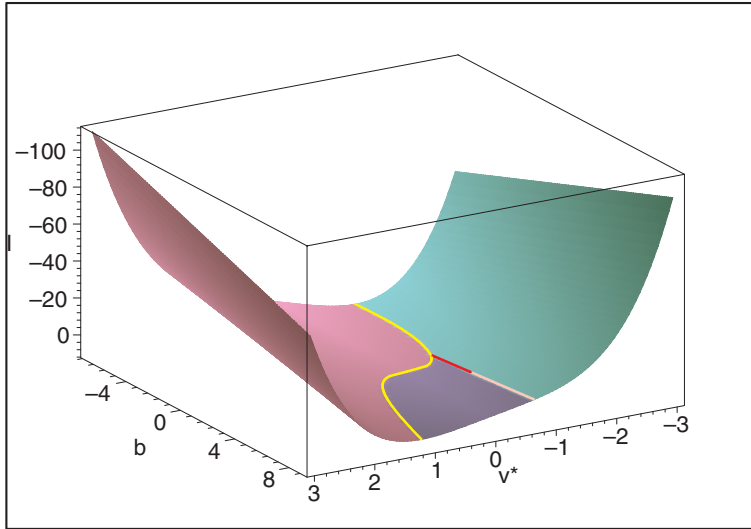


FIG. 3.1. v fixed points and their stability in function of I and b . The reddish/pinkish component is the surface of saddle fixed points, the purplish one corresponds to the repulsive fixed points, and the bluish/greenish one corresponds to the attractive fixed points. The yellow curve corresponds to a saddle-node bifurcation, the red curve to a subcritical Andronov–Hopf bifurcation, and the greyish one to the supercritical Andronov–Hopf bifurcation. The intersection point between the yellow and the red curve is the Bogdanov–Takens bifurcation point, and the intersection point of the red and greyish curves is the Bautin bifurcation point.

- When $b < \frac{5}{2}a$, then $\alpha > 0$, hence $l_1 > 0$, and the Andronov–Hopf bifurcation is subcritical.
- When $b > \frac{5}{2}a$, then $\alpha < 0$, hence $l_1 < 0$, and the Andronov–Hopf bifurcation is supercritical.

We prove below that the change in the type of Hopf bifurcation is obtained via a Bautin bifurcation.

- (B3) A Bogdanov–Takens bifurcation point is located at $b = a$ and $I = -3\left(\frac{a}{4}\right)^{(4/3)}$.
 (B4) A saddle homoclinic bifurcation curve satisfying, near the Bogdanov–Takens point, the equation

$$(P) := \left\{ \left(I = -3\left(\frac{a}{4}\right)^{(4/3)} + I_1, b = a + b_1 \right) ; \right. \\
 I_1 = \frac{1}{12} \left(-\frac{25}{6}a - \frac{37}{6}b_1 + \frac{5}{6} \sqrt{25a^2 + 74b_1a + 49b_1^2} \right) a^{1/3} \\
 + o(|b_1| + |I_1|) \\
 \left. \text{and } b_1 > -6I_1a^{-1/3} \right\}.$$

- (B5) A Bautin bifurcation at the point $(b = \frac{5}{2}a, I = -3\left(\frac{a}{4}\right)^{4/3}(2a - 1))$ and a saddle node bifurcation of periodic orbits coming along (see section 3.2).

Figure 3.1 represents the bifurcation curves and the fixed point of the quartic model in the space (I, b, v) .

3.2. The Bautin bifurcation. As we have seen in the last section, at the point

$$(3.2) \quad \begin{cases} v_a = -\left(\frac{a}{4}\right)^{1/3}, \\ I = -3\left(\frac{a}{4}\right)^{4/3}(2a-1), \\ b = \frac{5}{2}a \end{cases}$$

the Jacobian matrix of the system has a pair of purely conjugate imaginary eigenvalues and a vanishing first Lyapunov exponent.

To prove the existence of a Bautin bifurcation, we start our computations from the point of section 1.3.4. In this case the calculations can be led until the end, but the expressions are very intricate, and we do not reproduce it here. In Appendix A we show the calculations to perform. We prove that the system actually undergoes a Bautin bifurcation except for two particular values of the parameter a .⁴

With this method we obtain a closed-form expression for the second Lyapunov exponent. We show that this second Lyapunov exponent vanishes for two values of a , whose expressions are complicated. These calculations are rigorous, but nevertheless, the interested reader can find numerical expressions of this exponent to get a grasp on its behavior in the appendix (see (A.7)) and of the two numerical values of a such that $l_2(a)$ vanishes.

Things are even more involved when we are interested in the regularity of the map $(I, b) \mapsto (\mu(I, b), l_1(I, b))$. Nevertheless, we obtain that this determinant never vanishes.

Eventually, for all a different from the critical values where the second Lyapunov exponent vanishes, the system undergoes a Bautin bifurcation.

Note finally that the Bautin bifurcation point separates two branches of sub- and supercritical Hopf bifurcations. For nearby parameter values, the system has two coexisting limit cycles, an attractive one and a repelling one, which collide and disappear via a saddle-node bifurcation of periodic orbits.

4. Numerical simulations. In the previous sections we emphasized the fact that the class of models we defined in section 1 was able to reproduce the behaviors observed by Izhikevich in [15]. In this section, first we show that the quartic model indeed reproduces the behaviors observed by Izhikevich and which correspond to cortical neuron behaviors observed experimentally. We also produce some simulations of self-sustained subthreshold oscillations which occur only when the dynamical system has attracting periodic orbits, which is not the case in the IBG models.

Izhikevich in [15] explains the main features we obtain in numerical simulations from the neurocomputational point of view. In this paper, we comment on these same features from the dynamical systems point of view. This analysis also gives us a systematic way of finding the parameters associated with one of the possible behaviors.

4.1. Simulation results. We now provide simulation results of the quartic model introduced in section 3. In the simulated model, the spike is not represented by the blow up of the potential membrane v , but we consider that the neuron emits a spike when its membrane potential crosses a constant threshold.⁵

⁴All the computations have been performed using Maple, but the expressions are very involved and are not reproduced here.

⁵Note that the numerical simulations are very robust with respect to the choice of the threshold, if taken large enough, since the underlying equation blows up in finite time.

Let θ be our threshold. The simulated model considered in this section is the solution of the equations

$$(4.1) \quad \begin{cases} \dot{v} = v^4 + 2av - w + I, \\ \dot{w} = a(bv - w) \end{cases}$$

together with the spike-and-reset condition

$$(4.2) \quad \text{If } v(t^-) > \theta \Rightarrow \begin{cases} v(t) = v_r, \\ w(t) = w(t^-) + d. \end{cases}$$

Simulations have been done using an Euler numerical scheme, with a time step ranging from 10^{-1} to 10^{-2} depending on the precision needed, and with time intervals ranging from 10 to 500. This method is very efficient numerically and remains precise. Other integration methods could be used, and the qualitative results we obtained do not depend on the integration scheme, as soon as the time step is small enough.

REMARK (on Figure 4.1). *Note that we did not reproduce the last three behaviors presented by Izhikevich in [15, Figs. 1.(R), 1.(S), and 1.(T)]. Indeed, these behaviors are not in the scope of the present paper and do not correspond to the model we studied.*

More precisely, in the study of the general model (1.1), we considered for phenomenological reasons $a > 0$, modelling the leak of the adaptation variable: the adaptation would converge to its rest value if it was not influenced by the membrane potential v . If we considered $a < 0$, this adaptation variable would diverge exponentially from this rest value if it was not controlled by the membrane potential v . The inhibition-induced behaviors [15, Figs. 1.(S) and 1.(T)] require a to be strictly negative, and so we will not comment on these behaviors any further.

Similarly, the accommodation behavior presented by Izhikevich in [15, Fig. 1.(R)] is a limit case when w is very slow and the adaptation efficiency b very high. Mathematically speaking, it corresponds to a case where $a \rightarrow 0$ and $ab \rightarrow \lambda \neq 0$. This case is not taken into account in our study and amounts to replacing (1.1) by an equation of the type

$$(4.3) \quad \begin{cases} \frac{dv}{dt} = F(v) - w + I, \\ \frac{dw}{dt} = ab(v - v_0), \end{cases}$$

and the study of this equation is not in the scope of the present paper.

The simulated behaviors we obtained in Figure 4.1 have been obtained playing with the bifurcation parameters in the phase plane. The way the parameters were set was based on a qualitative reasoning on the phase plane and the bifurcation diagram in a way we now describe.

4.2. Bifurcations and neuronal dynamics. In this section we link the neuronal behaviors shown in Figure 4.1 with the bifurcations of the system.

- (i) *Tonic spiking:* This behavior corresponds to the saddle-node bifurcation. The system starts from a (stable) equilibrium point near the saddle-node bifurcation curve (see Figure 4.2). Then we apply a greater constant current I , and the new dynamical system has no fixed point (we “cross” the saddle-node bifurcation curve). So the neuron begins spiking. The stabilization of the spiking frequency is linked with the existence of what we will call a *limit spiking cycle*. Indeed, we can see that the phase plane trajectory

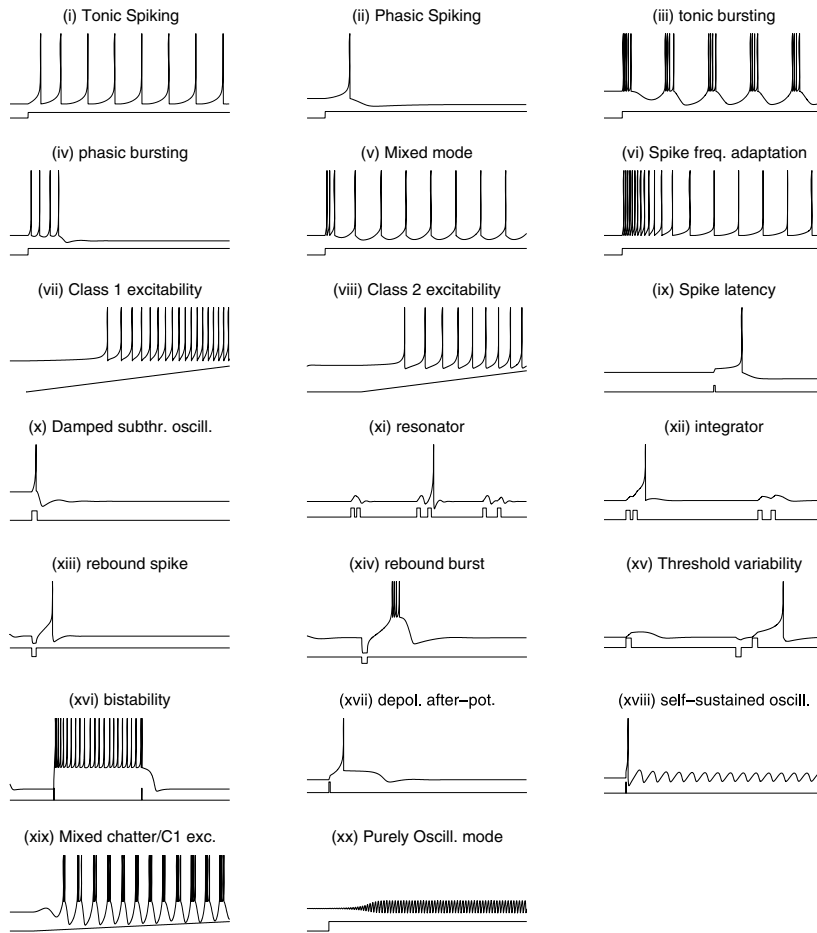


FIG. 4.1. Different remarkable neurocomputational interesting behaviors of the neuron model (4.1) with the reset condition (4.2) for different choices of the parameters (a, b, I, v_r, d) . The higher curve represents the membrane potential v and the lower one the input current I (see Appendix B for the numerical values of each simulations).

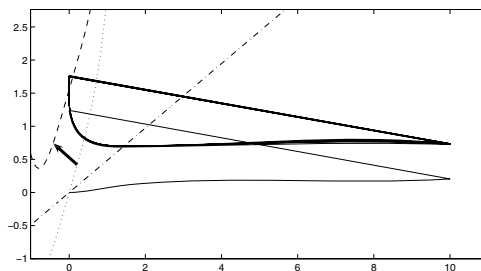


FIG. 4.2. Tonic spiking: phase plane trajectory. The dotted curve is the v nullcline at the initial time. It is shifted to the dashed one when applying a constant input current. The new dynamical system has no fixed point and spikes regularly. We can see the spiking cycle appearing.

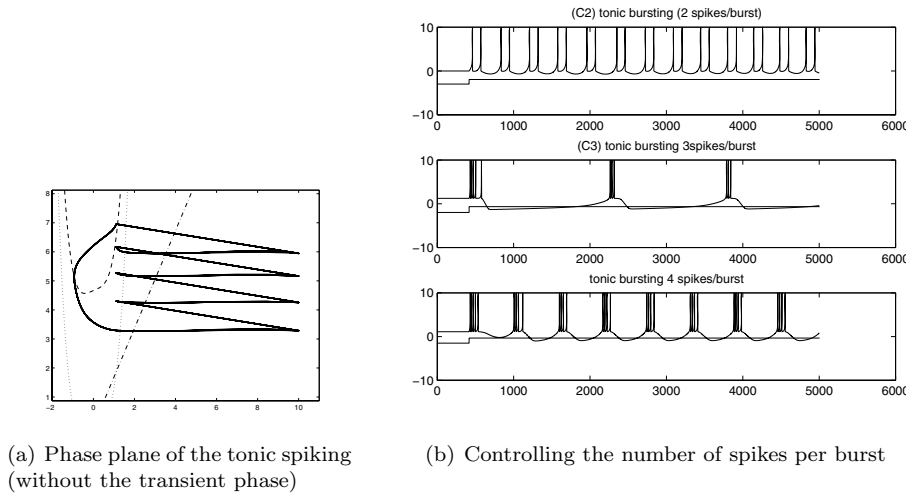


FIG. 4.3. *Tonic bursting: phase plane trajectory. The dotted curve is the v nullcline at the initial time. It is shifted to the dashed one when applying a constant input current. The new dynamical system has no fixed point. We can see the multiple spike limit cycle here.*

converges to a kind of cycle. This cycle includes a spike point ($v = \infty$, or $v = \text{threshold}$ in the numerical case), and so it is not a classical limit cycle. The v is always reset to the same value, and we can see that the adaptation variable w converges to an attracting stable value w_{spike} . This value satisfies $w_s(t_{\text{spike}}) + b = w_{\text{spike}}$, where $w_s(\cdot)$ is solution of (4.1) with the initial conditions

$$\begin{cases} v(0) = v_r, \\ w(0) = w_{\text{spike}} \end{cases}$$

and where t_{spike} denotes the time of the spike.

- (ii) *Phasic spiking*: This behavior occurs on the stable fixed point portion of the phase plane. The system starts at a fixed point. Then we apply a constant current to the neuron greater than the initial current but lower than the current associated with the saddle-node bifurcation. This stimulation forces the neuron to spike. Nevertheless, the reset point falls in the attraction basin of the new fixed point, and the trajectory converges to this point.
- (iii) *Tonic bursting*: This behavior is also linked to the saddle-node bifurcation. The system starts at a (stable) fixed point, and when we apply a constant current, we cross this bifurcation. The new dynamical system has no fixed point and is in a spiking behavior. The only difference with the tonic spiking behavior is that the point (v_r, w_{spike}) is in the zone $\{(v, w); \dot{v} < 0\}$. So the system emits quickly a precise number of spikes and then crosses the v nullcline. At this point, the membrane potential decays before spiking. We can see numerically that the system converges to a stable *spiking cycle* (see Figure 4.3(a)) containing a given number of spikes, a decay, and then the same sequence of spikes again. So the two-dimensional system is able to reproduce the diagrams presented by Izhikevich in [13] in an (at least) three-dimensional space. This is possible in two dimensions because of the

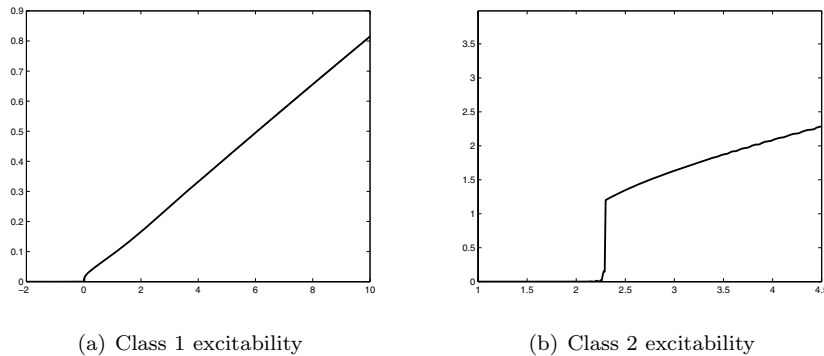
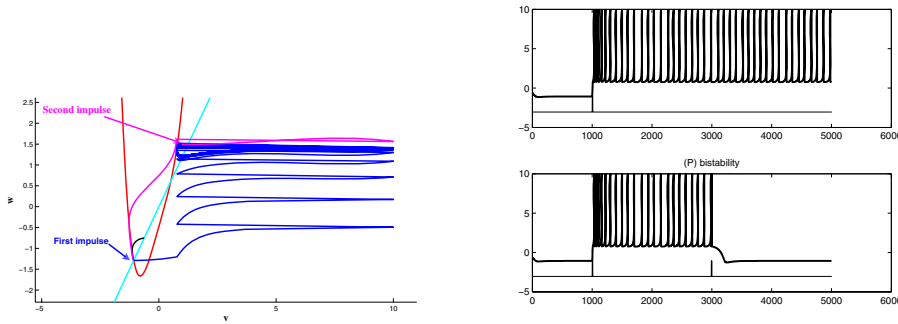


FIG. 4.4. *Spiking frequency vs. input current I for different choices of b . These curves have been obtained running simulations for different values of the input current, computing the frequency of the emitted spikes in a time range $T = 10000$.*

singularity of the model (explosion or threshold/reinitialization). If the system was regular, this behavior would not have been possible because it would have contradicted the Cauchy–Lipschitz theorem of existence and uniqueness of a solution.

Note that we can choose exactly the number of spikes per burst by changing the adaptation parameter d and that the bursting can be of parabolic or square-wave type as defined in Hoppensteadt and Izhikevich [12] (see Figure 4.3(b)).

- (iv) *Phasic bursting*: This behavior is linked with what we discussed in (ii) and (iii): the system starts at a stable fixed point. When the input current is turned on, the nullcline is shifted and the initial point is now in the spiking zone, and so a spike is emitted. Nevertheless, in contrast with (ii), the reset does not fall in the attraction basin of the new stable fixed point, but the point (v_0, w_{spike}) is inside this attraction basin. So a certain number of spikes are emitted before returning to the new fixed point. Here again we are able to control the number of spikes in the initial burst.
- (v) *Mixed mode*: The dynamical system interpretation is mixed between the phasic bursting and the tonic spiking. A certain number of spikes are necessary to converge to the spiking cycle.
- (vi) *Spike frequency adaptation*: This behavior is a particular case of tonic bursting where the convergence to the stable spiking cycle is slow.
- (vii)/(viii) *Class one/two excitability*: Figure 4.4(a) and (b) represents the spiking frequency of the neurons as a function of the input current. We can see that for the first choice of parameter, the frequency can be very small and increases regularly, and for the second choice of parameter, we can see that the system cannot spike in a given range of frequency (this frequency cannot be lower than 1.2Hz). Those simulations show that, depending on the chosen parameters, the system can be class 1 or class 2 excitable.
- (ix)/(xvii) *Spike latency/DAP*: It is a particular case of phasic spiking when the equilibrium v^* or the reset point v_r is near a point such that $F(v) = F'(v) = 0$. The membrane potential dynamics is very slow around this point. In the spike latency behavior, the initial point is close to this point, which generates the observed latency. In our case, it is around the minimum of



(a) Bistability: return to equilibrium via the same impulse

(b) Bistability

FIG. 4.5. *Bistability phenomenon: The first impulse induces a self-sustained tonic spiking behavior while the system has a stable fixed point. The second impulse perturbs this regular spiking behavior, and the system falls in the attraction basin of the stable fixed point.*

the function F (see Figure 4.6(ix)). In the depolarized after-potential (DAP) case, the reset occurs near this point, which is also in the attraction basin of the stable fixed point.

- (x) *Damped subthreshold oscillations*: This behavior occurs in the neighborhood of the stable fixed point: the stimulation evokes a spike, and the reset falls in the attraction basin of the stable fixed point, which has complex eigenvalues with negative real parts. This generates damped subthreshold oscillations.
- (xi) *Resonator*: This behavior occurs at the stable fixed point when the Jacobian matrix has complex eigenvalues. The first spike induces damped subthreshold oscillations. The spike is emitted if the second spike is given at the period of those oscillations, which is given by the argument of the complex eigenvalue. If it occurs before or after, then no spike is emitted.
- (xii) *Integrator*: This behavior occurs when we stimulate the system from the stable fixed point when the Jacobian matrix has real (negative) eigenvalues. If the first stimulation is not sufficient to make the neuron spike, then the stimulation is damped. Nevertheless, the membrane potential returns to equilibrium slowly, and if the same stimulation arrives to the “destabilized” neuron, it can generate a spike. The closer the second stimulation is to the first one, the more probable the omission of the spike.
- (xiii)/(xiv) *Rebound spike or burst*: The input impulse makes the neuron spike, and the reset (or the second, third, n th reset) falls in the attraction basin of the stable fixed point.
- (xv) *Threshold variability*: This phenomenon is exactly the same as the integrator, but instead of destabilizing the variable v we play on the adaptation variable.
- (xvi) *Bistability*: This behavior starts from the stable fixed point. The *attracting reset* (v_r, w_{spike}) is outside the attraction basin of the fixed point but still close to this zone. The first impulse generates a spike and initiates a tonic spiking mode. Nevertheless, it is possible via a small perturbation of the trajectory to fall into the attraction basin of the fixed point (see Figure 4.5).

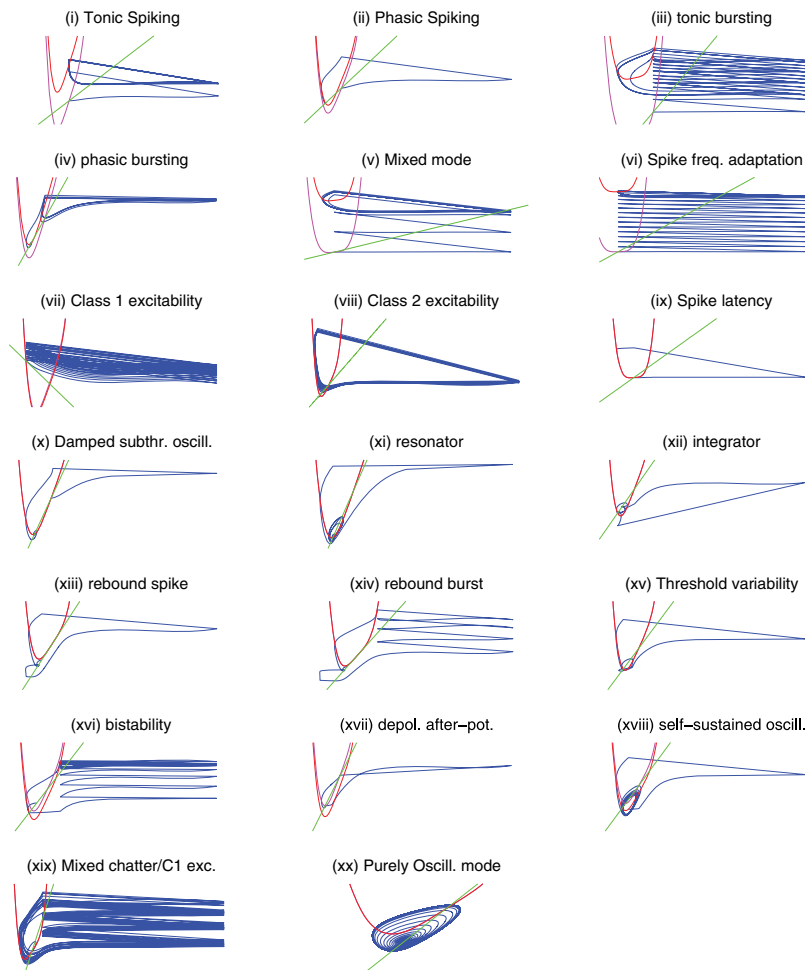


FIG. 4.6. Phase diagrams corresponding to the behaviors presented in Figure 4.1.

- (xviii)/(xx) *Self-sustained subthreshold oscillations and purely oscillating mode*: They are linked with the supercritical Hopf bifurcation and its stable periodic orbit. These two behaviors cannot be obtained in the IBG models since the Hopf bifurcations are always subcritical.

4.3. Self-sustained subthreshold oscillations in cortical neurons. In this study we gave a set of sufficient conditions to obtain an IBG-like model of neuron. In this framework we proposed a model that displays a Bautin bifurcation the IBG neurons lack; as a consequence our model can produce subthreshold oscillations. In this section, we explain from a biological point of view the origin and the role of those oscillations and reproduce in vivo recordings.

In the IBG models, the Andronov–Hopf bifurcation is always subcritical. The only oscillations created in these models are damped (see Figure 4.7(a)) and correspond in the phase plane to the convergence to a fixed point where the Jacobian matrix has complex eigenvalues. Our quartic model undergoes supercritical Andronov–Hopf bifurcations, and so there are attracting periodic solutions. This means that the

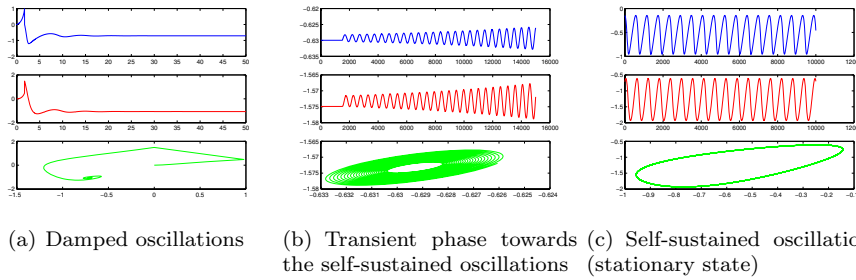


FIG. 4.7. The quartic model shows damped subthreshold oscillations like the IBG models (Figure 4.7(a)): the trajectory collapses to a fixed point (parameters: $a = 1$, $b = 1.5$, $I = 0.1$, $T_{max} = 100$, $dt = 0.01$). The upper (blue) curve represents the solution in v , the middle (red) one w , and the lower one (green) the trajectory in the plane (v, w). Self-sustained subthreshold oscillations of the quartic model (Figures 4.7(b) and 4.7(c)): the trajectory is attracted towards a limit cycle (parameters: $a = 1$, $b = 5/2$, $I = -3(a/4)^{4/3}(2a-1)$, $T_{max} = 150000$, $dt = 0.01$, $I = (-3(a/4)^{4/3}(2a-1) + 0.001)$.

neurons can show self-sustained subthreshold oscillations (Figures 4.7(b) and 4.7(c)), which is of particular importance in neuroscience.

Most biological neurons show a sharp transition from silence to a spiking behavior, which is reproduced in all the models of class (1.1). However, experimental studies suggest that some neurons may experience a regime of small oscillations [21]. These subthreshold oscillations can facilitate the generation of spike oscillations when the membrane gets depolarized or hyperpolarized [22, 23]. They also play an important role in shaping specific forms of rhythmic activity that are vulnerable to the noise in the network dynamics.

For instance, the inferior olive nucleus, a part of the brain that sends sensory information to the cerebellum, is composed of neurons able to support oscillations around the rest potential. It has been shown by Llinás and Yarom [22, 23] that the precision and robustness of these oscillations are important for the precision and the robustness of spike generation patterns. The quartic model is able to reproduce the main features of the inferior olive neuron dynamics:

- i. autonomous subthreshold periodic and regular oscillations (see intracellular recordings of inferior olive neurons in brain stem slices in [23]),
- ii. rhythmic generation of action potentials.

The robust subthreshold oscillations shown by in vivo recordings [4, 21, 23] correspond in our quartic model to the stable limit cycle coming from the supercritical Hopf bifurcation. The oscillations generated by this cycle are stable, and they have a definite amplitude and frequency. This oscillation occurs at the same time as the rhythmic spike generation in the presence of noisy or varying input. Note that other neuron models such as those studied above, even if they do not undergo a supercritical Hopf bifurcation, can also exhibit oscillations in the presence of noise, for instance near a subcritical Hopf bifurcation. Nevertheless, these oscillations do not have the regularity in the amplitude and the frequency linked with the presence of an attracting limit cycle. The results we obtain simulating the quartic model are very similar to those obtained by in vivo recordings (see Figure 4.8).

But the inferior olive neurons are not the only neurons to present subthreshold membrane potential oscillations. For instance, stellate cells in the entorhinal cortex demonstrate theta frequency subthreshold oscillations [1, 2, 17], linked with the persistent Na^+ current I_{NaP} .

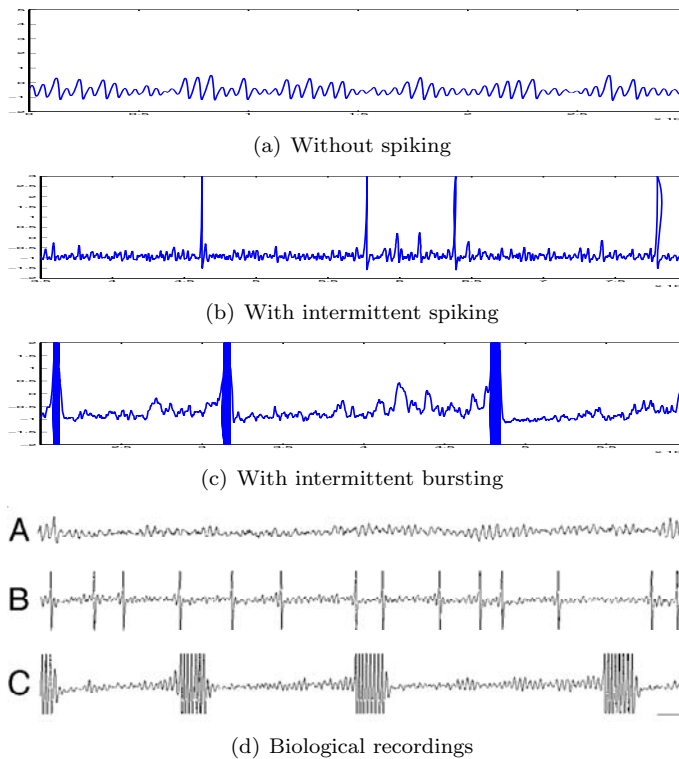


FIG. 4.8. *Subthreshold membrane oscillations, qualitatively reproducing the recordings from [20] in DRG neurons. Traces illustrate (4.8(a)) oscillations without spiking, (4.8(b)) oscillations with intermittent spiking, and (4.8(c)) oscillations with intermittent bursting (in the figures, spikes are truncated). The noisy input is an Ornstein–Uhlenbeck process. The biological recordings 4.8(d) are reproduced from [20, Fig. 1] and used with permission.*

We now conclude this section on the specific example of subthreshold self-sustained oscillations given by the dorsal root ganglia (DRG) neuron. This neuron presents subthreshold membrane potential oscillations coupled with repetitive spike discharge or burst, for instance in the case of a nerve injury [20, 3]. Figure 4.8(d) shows biological *in vivo* intracellular recordings performed by Liu et al. [20] from a DRG neuron of an adult male rat. The recorded membrane potentials exhibit high frequency subthreshold oscillation in the presence of noise, combined with a repetitive spiking or bursting. These behaviors can be reproduced by the quartic model, as we can see in Figure 4.8, around a point where the system undergoes a supercritical Hopf bifurcation.⁶

Conclusion. In this paper we defined a general class of neuron models able to reproduce a wide range of neuronal behaviors observed in experiments on cortical neurons. This class includes the Izhikevich and the Brette–Gerstner models, which are widely used. We derived the bifurcation diagram of the neurons of this class and proved that they all undergo the same types of bifurcations: a saddle-node bifurcation curve, an Andronov–Hopf bifurcation curve, and a codimension two Bogdanov–Takens

⁶The amplitude and frequency of the subthreshold oscillations can be controlled choosing a point on the supercritical Hopf bifurcation curve.

bifurcation. We proved that there was only one other possible fixed-point bifurcation, a Bautin bifurcation. Then using those theoretical results we proved that the Izhikevich and the Brette–Gerstner models had the same bifurcation diagram.

This theoretical study allows us to search for interesting models in this class of neurons. Indeed, Theorem 1.9 ensures us that the bifurcation diagram will present at least the bifurcations stated. This information is of great interest if we want to control the subthreshold behavior of the neuron of interest.

Following these ideas, we introduced a new neuron model of our global class undergoing the Bautin bifurcation. This model, called the *quartic model*, is computationally and mathematically as simple as the IBG models and able to reproduce some cortical neuron behaviors which the IBG models cannot reproduce.

This study focused on the subthreshold properties of this class of neurons. The adaptative reset of the model is of great interest and is a key parameter in the repetitive spiking properties of the neuron. Its mathematical study is very rich and is still an ongoing work.

Appendix A. Bautin bifurcation. In this appendix we prove that the quartic model undergoes a Bautin bifurcation at the point

$$(A.1) \quad \begin{cases} b = \frac{5}{2}a, \\ I = -3\left(\frac{a}{4}\right)^{4/3}(2a-1), \\ v_a = -\left(\frac{a}{4}\right)^{1/3}. \end{cases}$$

A.1. The first Lyapunov exponent. Indeed, using a suitable affine change of coordinates, the system at this point reads

$$(A.2) \quad \begin{cases} \dot{x} = \omega y, \\ \dot{y} = \frac{ab}{\omega} (6v_a^2 v_1(x, y)^2 + 4v_a v_1(x, y)^3 + v_1(x, y)^4) \\ \quad = \frac{1}{2}F_2\left(\begin{pmatrix} x \\ y \end{pmatrix}, \begin{pmatrix} x \\ y \end{pmatrix}\right) + \frac{1}{6}F_3\left(\begin{pmatrix} x \\ y \end{pmatrix}, \begin{pmatrix} x \\ y \end{pmatrix}, \begin{pmatrix} x \\ y \end{pmatrix}\right) + \frac{1}{24}F_4\left(\begin{pmatrix} x \\ y \end{pmatrix}, \begin{pmatrix} x \\ y \end{pmatrix}, \begin{pmatrix} x \\ y \end{pmatrix}, \begin{pmatrix} x \\ y \end{pmatrix}\right), \end{cases}$$

where $v_1(x, y) = \frac{1}{b}x + \frac{\omega}{ab}y$. We also denote $F_2(X, Y)$, $F_3(X, Y, Z)$, and $F_4(X, Y, Z, T)$ the multilinear symmetric vector functions of (A.2) ($X, Y, Z, T \in \mathbb{R}^2$):

$$\begin{cases} F_2\left(\begin{pmatrix} x \\ y \end{pmatrix}, \begin{pmatrix} z \\ t \end{pmatrix}\right) = \begin{pmatrix} 0 \\ 12\frac{ab}{\omega}v_a^2v_1(x, y)v_1(z, t) \end{pmatrix}, \\ \dots \end{cases}$$

To compute the two first Lyapunov exponents of the system, we follow Kuznetsov’s method [19]. In this method we need to compute some specific right and left complex eigenvectors, which can be chosen in our case to be

$$(A.3) \quad \begin{cases} p = \begin{pmatrix} \frac{1}{-i\sqrt{a}b-a^2+a} \\ 1 \end{pmatrix}, \\ q = \begin{pmatrix} \frac{1}{2} \frac{(i\sqrt{a(b-a)}+a)b}{b-a-i\sqrt{a(b-a)}} \\ 1/2 \frac{(i\sqrt{a(b-a)}+a)^2}{a(b-a-i\sqrt{a(b-a)})} \end{pmatrix}. \end{cases}$$

We now put the system in a complex form letting $z = x + iy$.

We can now compute the complex Taylor coefficients g_{ij} :

$$(A.4) \quad \begin{cases} g_{20} = \langle p, F_2(q, q) \rangle, \\ g_{11} = \langle p, F_2(q, \bar{q}) \rangle, \\ g_{02} = \langle p, F_2(\bar{q}, \bar{q}) \rangle, \\ \\ g_{30} = \langle p, F_3(q, q, q) \rangle, \\ g_{21} = \langle p, F_3(q, q, \bar{q}) \rangle, \\ g_{12} = \langle p, F_3(\bar{q}, \bar{q}, \bar{q}) \rangle, \\ g_{03} = \langle p, F_3(\bar{q}, \bar{q}, \bar{q}) \rangle, \\ \dots \end{cases}$$

So the Taylor coefficients (A.4) read

$$(A.5) \quad \begin{cases} g_{20} = 12 \frac{ab}{\omega} v_a^2 v_1 \left(\frac{1}{2} \frac{(i\sqrt{a(b-a)}+a)b}{b-a-i\sqrt{a(b-a)}}, \frac{1}{2} \frac{(i\sqrt{a(b-a)}+a)^2}{a(b-a-i\sqrt{a(b-a)})} \right)^2, \\ g_{11} = 12 \frac{ab}{\omega} v_a^2 v_1(q)v_1(\bar{q}), \\ g_{02} = 12 \frac{ab}{\omega} v_a^2 v_1(\bar{q})v_1(\bar{q}), \\ \dots \end{cases}$$

Now let $S(I, b) := F'(v_-(I, b))$ be the value of the derivative of the function F , defined around the bifurcation point we are interested in.

The Jacobian matrix in the neighborhood of the point (A.1) reads

$$L(v) = \begin{pmatrix} S(I, b) & 1 \\ ab & -a \end{pmatrix}.$$

Let us denote $\alpha = \begin{pmatrix} I \\ b \end{pmatrix}$ the parameter vector and $\lambda(\alpha) = \mu(\alpha) \pm i\omega(\alpha)$ the eigenvalues of the Jacobian matrix. We have

$$\begin{cases} \mu(\alpha) = \frac{1}{2} (S(\alpha) - a), \\ \omega(\alpha) = \frac{1}{2} \sqrt{-(S(\alpha) - a)^2 + 4ab}. \end{cases}$$

With these notations, let $c_1(\alpha)$ be the complex defined by

$$c_1(\alpha) = \frac{g_{20}g_{11}(2\lambda + \bar{\lambda})}{2|\lambda|^2} + \frac{|g_{11}|^2}{\lambda} + \frac{|g_{02}|^2}{2(2\lambda - \bar{\lambda})} + \frac{g_{21}}{2}$$

(in this formula we omit the dependence in α of λ for the sake of clarity).

The first Lyapunov exponent $l_1(\alpha)$ eventually reads

$$(A.6) \quad \boxed{l_1(\alpha) = \frac{Re(c_1(\alpha))}{\omega(\alpha)} - \frac{\mu(\alpha)}{\omega(\alpha)^2} Im(c_1(\alpha))}$$

A.2. The second Lyapunov exponent. The method to compute the second Lyapunov exponent is the same as the one we described in the previous section. The expression is given by the following formula:

$$\begin{aligned}
 2l_2(0) = & \frac{1}{\omega(0)} \operatorname{Re}[g_{32}] \\
 & + \frac{1}{\omega(0)^2} \operatorname{Im} \left[g_{20} \bar{g}_{31} - g_{11} (4 g_{31} + 3 \bar{g}_{22}) - \frac{1}{3} g_{02} (g_{40} + \bar{g}_{13}) - g_{30} g_{12} \right] \\
 & + \frac{1}{\omega(0)^3} \left\{ \operatorname{Re} \left[g_{20} \left(\bar{g}_{11} (3 g_{12} - \bar{g}_{30}) + g_{02} (\bar{g}_{12} - 1/3 g_{30}) + \frac{1}{3} \bar{g}_{02} g_{03} \right) \right. \right. \\
 & \left. \left. + g_{11} \left(\bar{g}_{02} \left(\frac{5}{3} \bar{g}_{30} + 3 g_{12} \right) + \frac{1}{3} g_{02} \bar{g}_{03} - 4 g_{11} g_{30} \right) \right] \right. \\
 & \left. + 3 \operatorname{Im}[g_{20} g_{11}] \operatorname{Im}[g_{21}] \right\} \\
 & + \frac{1}{\omega(0)^4} \left\{ \operatorname{Im} [g_{11} \bar{g}_{02} (g_{20}^2 - 3 \bar{g}_{20} g_{11} - 4 g_{11}^2)] \right. \\
 & \left. + \operatorname{Im}[g_{20} g_{11}] (3 \operatorname{Re}(g_{20} g_{11}) - 2 |g_{02}|^2) \right\}.
 \end{aligned}$$

This expression is quite intricate in our case. Nevertheless, we have a closed-form expression depending on the parameter a , vanishing for two values of the parameter a . We evaluate numerically this second Lyapunov exponent. We get the following expression:

$$\begin{aligned}
 l_2(a) \approx & -0.003165 a^{-\frac{28}{3}} - 0.1898 a^{-\frac{22}{3}} + 0.3194 a^{-16/3} \\
 \text{(A.7)} \quad & - 0.05392 a^{-\frac{25}{3}} + 0.1400 a^{-\frac{19}{3}} - 0.3880 a^{-7/3} + 0.5530 a^{-10/3} \\
 & + 0.7450 a^{-13/3}.
 \end{aligned}$$

We can see that this numerical exponent vanishes only for two values of the parameter a which are

$$\{0.5304, 2.385\}.$$

The expression of the determinant of the matrix $D_{I,b}(\mu(I, b), l_1(I, b))$ is even more involved, and so we do not reproduce it here (it would take pages to write down its numerical expression!). Nevertheless, we proceed exactly as we did for the second Lyapunov exponent and obtain again the rigorous result that this determinant never vanishes for all $a > 0$.

Appendix B. Numerical values for the simulations. In this annex we give the numerical values used to generate Figure 4.1.

| | | |
|--|---|---|
| (i) Tonic Spiking $a = 1; b = 0.49; v_r = 0;$ $I(t) = 1.56\mathbb{1}_{t>1}(\theta); d = 1;$ $T = 10; dt = 0.01; \theta = 10;$ | (ii) Phasic Spiking $a = 1; b = 0.76; v_r = 0.2;$ $I(t) = 0.37\mathbb{1}_{t>1}(\theta); d = 1;$ $T = 10; dt = 0.01; \theta = 10;$ | (iii) Tonic Bursting $a = 0.15; b = 1.68; v_r = (-2a + b)\frac{1}{3};$ $I(t) = 4.67\mathbb{1}_{t>1}(\theta); d = 1;$ $T = 30; dt = 0.01; \theta = 10;$ |
| (iv) Phasic Bursting $a = 1.58; b = 1.70; v_r = -\frac{a}{3};$ $I(t) = 0.73\mathbb{1}_{t>1}(\theta); d = 0.01;$ $T = 50; dt = 0.01; \theta = 10.$ | (v) Mixed Mode $a = 0.07; b = 0.32; v_r = 0;$ $I(t) = 3.84\mathbb{1}_{t>1}(\theta); d = 1.50;$ $T = 50; dt = 0.01; \theta = 10.$ | (vi) Spike Freq. Adaptation $a = 0.02; b = 0.74; v_r = 0;$ $I(t) = 4.33\mathbb{1}_{t>1}(\theta); d = 0.36;$ $T = 50; dt = 0.01; \theta = 10.$ |
| (vii) Class 1 Excitability $a = 4; b = 0.67; v_r = -1.3;$ $I(t) = -0.1 + 0.23t; d = 1;$ $T = 30; dt = 0.01; \theta = 10.$ | (viii) Class 2 Excitability $a = 1; b = 1.09; v_r = -1.2;$ $I(t) = 0.06t; d = 5;$ $T = 50; dt = 0.01; \theta = 20.$ | (ix) Spike Latency $a = 0.02; b = 0.42; v_r = 0;$ $I(t) = 5\delta_{7.5}(t); d = 1;$ $T = 15; dt = 0.01; \theta = 10.$ |
| (x) Damped Subthr. Oscill. $a = 2.58; b = 4.16; v_r = 0.1;$ $I(t) = 2\delta_2(t); d = 0.05;$ $T = 20; dt = 0.01; \theta = 10.$ | (xi) Resonator $a = 5.00; b = 7.88; v_r = -1.28;$ $I(t) = \delta_{6,6.8,15,16.5,24,26}(t); d = 0.5;$ $T = 30; dt = 0.01; \theta = 10.$ | (xii) Integrator $a = 1.00; b = 1.10; v_r = -0.97;$ $I(t) = \delta_{2.5,3.3,17.5,19}(t); d = 0.5;$ $T = 25; dt = 0.01; \theta = 10.$ |
| (xiii) Rebound Spike $a = 1; b = 2; v_r = -0.63;$ $I(t) = -0.48 - 5\delta_{2.5}(t); d = 1;$ $T = 50; dt = 0.1; \theta = 10.$ | (xiv) Rebound Burst $a = 1; b = 2; v_r = 1.3;$ $I(t) = -0.48 - 30\delta_{6.5}(t); d = 1;$ $T = 20; dt = 0.01; \theta = 10.$ | (xv) Threshold variability $a = 1; b = 1.23; v_r = -0.91;$ $I(t) = \delta_{2,16.5} - \delta_{15}; d = 1;$ $T = 20; dt = 0.01; \theta = 10.$ |
| (xvi) Bistability $a = 1; b = 1.2; v_r = 0.8;$ $I(t) = -0.47 + 20 * (\delta_{10} - \delta_{30}); d = 0.5;$ $T = 50; dt = 0.01; \theta = 10.$ | (xvii) Depol. after-pot $a = 1; b = 1.5; v_r = 0.06;$ $I(t) = 2\delta_3; d = 0.01;$ $T = 30; dt = 0.01; \theta = 10.$ | (xviii) Self-sustained oscill. $a = 1; b = 2.5; v_r = -0.63;$ $I(t) = -0.475 + 10 * \delta_{10}; d = 1;$ $T = 100; dt = 0.01; \theta = 10.$ |
| (xix) Mixed Chatter/ C^1 exc. $a = 0.89; b = 3.65; v_r = 1.12;$ $I(t) = 0.07t; d = 1;$ $T = 50; dt = 0.01; \theta = 10.$ | (xx) Purely oscill. $a = 1; b = 2.6; v_r = -0.63;$ $I(t) = -0.47\mathbb{1}_{t>1}; d = 1;$ $T = 500; dt = 0.01; \theta = 10.$ | |

REMARK. The $\delta_u(t)$ function is defined by

$$\delta_{u_1, \dots, u_N}(t) = \begin{cases} 1 & \text{if } t \in \bigcup_{k \in \{1, \dots, N\}} [u_k, u_k + 0.3], \\ 0 & \text{else.} \end{cases}$$

Acknowledgments. The author warmly acknowledges T. Viéville, B. Cessac, and Olivier Faugeras for fruitful discussions and suggestions.

REFERENCES

- [1] A. ALONSO AND R. KLINK, *Differential electroresponsiveness of stellate and pyramidal-like cells of medial entorhinal cortex layer II*, J. Neurophysiol., 70 (1993), pp. 128–143.
- [2] A. ALONSO AND R. LLINÁS, *Subthreshold Na⁺-dependent theta-like rhythmicity in stellate cells of entorhinal cortex layer II*, Nature, 342 (1989), pp. 175–177.
- [3] R. AMIR, M. MICHAELIS, AND M. DEVOR, *Membrane potential oscillations in dorsal root ganglion neurons: Role in normal electrogenesis and neuropathic pain*, J. Neurosci., 19 (1999), pp. 8589–8596.
- [4] L. S. BERNARDO AND R. E. FOSTER, *Oscillatory behavior in inferior olive neurons: Mechanism, modulation, cell aggregates*, Brain Res. Bull., 17 (1986), pp. 773–784.
- [5] R. BRETTE AND W. GERSTNER, *Adaptive exponential integrate-and-fire model as an effective description of neuronal activity*, J. Neurophysiol., 94 (2005), pp. 3637–3642.
- [6] B. ERMENTROUT, M. PASCAL, AND B. GUTKIN, *The effects of spike frequency adaptation and negative feedback on the synchronization of neural oscillators*, Neural Comput., 13 (2001), pp. 1285–1310.
- [7] L. C. EVANS, *Partial Differential Equations*, Grad. Stud. Math. 19, AMS, Providence, RI, 1998.
- [8] W. GERSTNER AND W. M. KISTLER, *Spiking Neuron Models*, Cambridge University Press, Cambridge, UK, 2002.
- [9] J. GUCKENHEIMER AND P. J. HOLMES, *Nonlinear Oscillations, Dynamical Systems and Bifurcations of Vector Fields*, Appl. Math. Sci. 42, Springer-Verlag, New York, 1983.
- [10] B. GUTKIN, B. ERMENTROUT, AND A. REYES, *Phase-response curves give the responses of neurons to transient inputs*, J. Neurophysiol., 94 (2005), pp. 1623–1635.
- [11] A. L. HODGKIN AND A. F. HUXLEY, *A quantitative description of membrane current and its application to conduction and excitation in nerve*, J. Physiol., 117 (1952), pp. 500–544.
- [12] F. HOPPENSTEADT AND E. M. IZHIKEVICH, *Weakly Connected Neural Networks*, Springer-Verlag, New York, Secaucus, NJ, 1997.
- [13] E. M. IZHIKEVICH, *Neural excitability, spiking, and bursting*, Internat. J. Bifur. Chaos Appl. Sci. Engrg., 10 (2000), pp. 1171–1266.
- [14] E. M. IZHIKEVICH, *Simple model of spiking neurons*, IEEE Transactions on Neural Networks, 14 (2003), pp. 1569–1572.
- [15] E. M. IZHIKEVICH, *Which model to use for cortical spiking neurons?*, IEEE Trans. Neural Netw., 15 (2004), pp. 1063–1070.
- [16] E. M. IZHIKEVICH, *Dynamical Systems in Neuroscience: The Geometry of Excitability and Bursting*, MIT Press, Cambridge, MA, 2007.
- [17] R. S. G. JONES, *Synaptic and intrinsic properties of neurones of origin of the perforant path in layer II of the rat entorhinal cortex in vitro*, Hippocampus, 4 (1994), pp. 335–353.
- [18] C. KOCH AND I. SEGEV, EDS., *Methods in Neuronal Modeling: From Ions to Networks*, MIT Press, Cambridge, MA, 1998.
- [19] Y. KUZNETSOV, *Elements of Applied Bifurcation Theory*, 2nd ed., Springer-Verlag, New York, 1998.
- [20] C. LIU, M. MICHAELIS, R. AMIR, AND M. DEVOR, *Spinal nerve injury enhances subthreshold membrane potential oscillations in DRG neurons: Relation to neuropathic pain*, J. Neurophysiol., 84 (2000), pp. 205–215.
- [21] R. LLINÁS, *The intrinsic electrophysiological properties of mammalian neurons: Insights into central nervous system function*, Science, 242 (1988), pp. 1654–1664.
- [22] R. LLINÁS AND Y. YAROM, *Electrophysiology of mammalian inferior olivary neurones in vitro. Different types of voltage-dependent ionic conductances*, J. Physiol., 315 (1981), pp. 549–567.
- [23] R. LLINÁS AND Y. YAROM, *Oscillatory properties of guinea-pig inferior olivary neurones and their pharmacological modulation: An in vitro study*, J. Physiol., 376 (1986), pp. 163–182.
- [24] J. RINZEL AND B. ERMENTROUT, *Analysis of Neural Excitability and Oscillations*, MIT Press, Cambridge, MA, 1989.
- [25] J. A. WHITE, T. BUDDÉ, AND A. R. KAY, *A bifurcation analysis of neuronal subthreshold oscillations*, Biophys. J., 69 (1995), pp. 1203–1217.